Optical SETI at Princeton:
November 2001–April 2002

Natalie Deffenbaugh

Professor David T. Wilkinson, Advisor

a paper submitted in partial fulfillment
of the requirements for the degree
of
Bachelor of Arts in Physics
at Princeton University

29 April 2002

Revised 27 May 2002

This thesis represents my own work
in accordance with University regulations.

_____

Acknowledgments

I would first like to express my sincere gratitude to Professor Wilkinson. His understanding and expertise have shined time and again as he has shepherded me through a change in topic and an abysmal ignorance of electrical circuitry. Chip Coldwell at Harvard could practically be considered a co-author of The Paper; when there is a question about the computer program, one cannot do better than to ask the programmer. Professor Gill Knapp in Astrophysics is also deserving of thanks for her help in my research of stellar clusters. And of course, none of this would have been possible without the unfailing dedication of the volunteers at Fitz-Randolph who sacrifice their sleep to collect the data that I use.

Peter Farrell and Penna Rose have been more than understanding of my thesis throes and have made do with the levels of commitment that I could muster. To my friends, thank you for understanding when I tried to act like a hermit; my special thanks to Jen who wouldn't let me. Thanks also to everyone in and around the Physics Department for welcoming an interloper. I have enjoyed myself immensely and learned a lot, spherical cow jokes aside.

Finally, I thank my family who, for four years, have supported me in my pursuit of academic endeavors of which they have no knowledge whatsoever.

Abstract

This is the first paper written about the optical SETI experiment at the Fitz-Randolph Observatory at Princeton University. We begin by summarizing the rationale behind a search for extra-terrestrial signals in the form of high energy laser pulses. We follow with a discussion of the experimental apparatus used in simultaneous observations of individual stars at Princeton's and Harvard-Smithsonian's observatories and how to interpret the data that it produces.

The central portion of this thesis comprises a preliminary analysis of the data taken at Princeton since November 2001. Attention is given to presenting, elucidating, and, where possible, explaining the photoelectron events that we see. We discuss both the individual events and the event rates. By comparing the data with theoretical predictions, we discover a number of faults in voltage levels, circuit timing, and possibly in the alignment of the telescope at the Fitz-Randolph observatory. Where possible, results are discussed with reference to similar data taken at Harvard. We find that the kpps (kilo-photoelectrons per second) rates are problematic at both observatories, but that there is in Princeton's data at least a correlation with the visual magnitude of the stars we observe.

We analyze the possibility of observing stellar clusters, rather than individual stars, to increase the efficiency of our observations. In the calculations, attention is paid to cluster density, distance, and age in order to determine if globular and open clusters are reasonable sources of the signals we seek. Finally, based on the analyses of the paper, the conclusion offers some recommendations for action on the part of the Princeton observing team.

Contents

Chapter 1

Introduction

On the night of 1 November 2001, members of Princeton's optical SETI team at the Fitz-Randolph Observatory made their first simultaneous stellar observations with the Harvard–Smithsonian Oak Ridge Observatory outside of Boston. Using identical instruments affixed to each telescope, and observing the same target star at the same time, we hope to find and validate high energy laser signals from extra-terrestrial sources; hence the acronym "optical search for extra terrestrial intelligence." The theoretical motivations behind this effort are discussed in Chapter 2 of this thesis.

Chapter 3 is meant as a technical introduction to the experimental apparatus and will be of service to anyone wishing to analyze the gathered data. In it we turn to the instrument itself, the OSETI box, and the software that analyzes the data collected at the telescopes. In essence, we look for the arrival in a small segment of time ($\approx 10\,ns$) of a sufficient number of photons to be noticeable over the ambient starlight. These photons are converted to photoelectrons, which produce the voltage pulses that actually enter our circuit. We examine more closely the types of signals we expect to see, how observations are made and analyzed, and how the circuitry and the software are supposed to work together to weed out false events. A sample observation from the data log file is presented with an explanation of what each entry indicates.

Having acquired sufficient knowledge of the experiment, we turn in Chapter 4 to the data themselves. Examining a sample of observations from both Princeton and Harvard from November 2001 through February 2002, we draw conclusions about the

electronics governing the capture and recording of photoelectron events. In particular, by examining the nature of so-called "bad" coincidences in the OSETI box, we find that there are likely voltage imbalances and internal timing errors that adversely affect the data-taking at Princeton.

These conclusions are borne out to an extent by the kpps (kilo-photoelectron per second) rates produced by the system diagnostics. However, there is a discrepancy of four orders of magnitude between the kpps rates and the calculated photon arrival rates from observed stars. This attenuation can be examined in two parts, first a drop in two orders of magnitude between the amplification of the signal and the record made of it in the log (discussed in Section 4.2.1), and second a preliminary drop of two orders of magnitude between the light that we think is entering the telescope and the photoelectron pulses that enter the coincidence circuits (discussed in Section 4.2.2). The latter calls into question the alignment of the OSETI box with respect to the axis of the telescope. The final data analysis looks at the hit rates recorded by our detector with respect to calculations made using the Poisson distribution (derived crudely in Section 4.3.1 and exactly in Section 4.3.2). We will see, once again, that the rates we observe are even lower than calculations predict for accidental events.

In an effort to place more stars in our field of view and thus improve the efficiency with which we can view the thousands of candidate objects, Chapter 5 examines the possibility of observing not single stars, but portions of globular and open stellar clusters. Basic calculations are made of the stellar density of clusters, and we incorporate that data along with criteria such as cluster distance and age to assess the viability from our perspective of observations of clusters.

Chapter 2

Historical and Theoretical Background

2.1 History of SETI: motivations for the current experiment

In their seminal 1959 paper in *Nature*, Cocconi and Morrison presented the first quantitative analysis of what signals we might expect to detect from extra-terrestrial civilizations in our galaxy. Their initial assumptions mandated looking only in the radio frequencies: they suggested the regime from 1 MHz to 10 GHz [8]. This suggested range was based on arguments that higher and lower frequencies would be subject to atmospheric absorption and that gamma-ray and visible frequency signals would demand too much power to make them feasible. The authors reasoned that the signal transmitters would assume the most simplistic of detection devices, ones that wouldn't have to guess hard at ideal frequencies or have the angular resolution to distinguish between a star and a planet orbiting it: hence the need for transmitted signals to overcome both galactic and stellar backgrounds [8].

The feasibility of transmitting signals in the radio regime was based on the level of existing earth technology and the supposition that any civilization broadcasting signals would be at least as advanced as ours. In addition to the proposed guidelines governing

transmitted signals, Cocconi and Morrison also articulated certain standards for terrestrial observation, suggesting that we look particularly at the seven sun-like stars within $10\,ly$ of our sun and suggesting that frequencies in the vicinity of the $21\,cm$ (1.42 GHz) emission line of neutral hydrogen would be the most likely to yield results [8].

In this early paper discussing possible types and sources for extra-terrestrial signals and plausible detection scenarios on earth, we see the considerations that lie at the heart of any SETI experiment. First (and obviously) any evaluation of the plausibility of various transmitted signals is based on the technical capabilities of our own civilization. This is not hubristic. We are advanced enough to consider the possibility of equally advanced life elsewhere in the universe, hopefully in our own galaxy, and if we can conceive of rather sophisticated means of transmission and detection, so could someone else. This relative argument means that more transmission and detection scenarios have become plausible as our technologies have advanced in the last forty years, most notably the possibility of observing an optical signal, discussed further below.

Second, though the search has certainly been expanded beyond the limited radius that Cocconi and Morrison first proposed, we still look for signals that come from relatively nearby. This assumption is also explained rather obviously when we consider the transit time that any signal will have as it is broadcast across the galaxy. We would like both that the transmitter of the signal still exist when we receive the message and that we might send a reply that would be observed in its turn: the desire for a dialogue necessitates reasonably small interstellar distances. Townes distills this principle nicely: we wish to search "within a radius from the Earth which is small enough to be practical from a technical point of view but large enough to contain a substantial number of suitable stars where such civilizations might exist" [34]. Third, we make the assumption that any transmitted signal in the visual bandwidth must overcome galactic and/or stellar noise. Indeed, as we shall see, starlight is the primary obstacle to justifying searches in the optical frequencies, since much more power is required to broadcast the higher-energy optical signals (see Table 2.1).

Fourth, and perhaps most important, we assume that there is a high enough probability of extraterrestrial civilization to warrant any search at all. The first and most

	Wavelength, λ (m)	Frequency, ν (Hz)
Radio	$> 10^{-1}$	$< 3 \times 10^{9}$
Microwave	$10^{-3} - 10^{-1}$	$3 \times 10^{9} - 3 \times 10^{11}$
Infrared	$10^{-7} - 10^{-3}$	$3 \times 10^{11} - 3 \times 10^{14}$
Optical	$4 \times 10^{-7} - 7 \times 10^{-7}$	$4 \times 10^{14} - 7.5 \times 10^{14}$
Ultraviolet	$10^{-8} - 10^{-7}$	$3 \times 10^{14} - 3 \times 10^{16}$
X-rays	$10^{-11} - 10^{-8}$	$3 \times 10^{16} - 3 \times 10^{19}$
Gamma rays	$< 10^{-11}$	$> 3 \times 10^{19}$

Table 2.1: Approximate divisions of the electromagnetic spectrum. The optical wavelengths, from about 400 to 700 nm, are a tiny fraction of the larger infrared bandwidth. Table compiled with data from [20].

authoritative attempt to quantize the number of advanced civilizations in our galaxy was presented by F.D. Drake in 1961 in the form of the equation that now bears his name. The number depends on seven parameters: the rate of formation of sun-like stars, the fraction thereof with planetary systems, the number of earth-like planets per typical system, the fraction of those planets where life will develop, the fraction of that life that can be considered intelligent, the fraction of those civilizations that will broadcast signals of any kind into space, and finally the length of time that a civilization broadcasts signals into space [19]. We can only guess at most of these numbers, but the sheer number of stars, and even sun-like stars, in our galaxy is enough to justify the endeavor; the current Harvard–Smithsonian-Princeton optical SETI project plans to observe more than 11,000 sun-like stars, all within 100 pc (326 ly) [28].

2.2 Optical SETI

Not long after Cocconi and Morrison's article, *Nature* published a piece that presented the possibility that civilizations more advanced than ours might use optical frequency masers, now called lasers, as a means of communication (the acronym stands for "Light Amplification by Stimulated Emission of Radiation") [32]. Detection of laser sighals would be possible with existing optical telescopes, and Schwartz and Townes presented analyses of various configurations of these optical masers, singly or in groups, that would produce a detectable optical signal at some distance from the transmitter. Because laser technology was so new at the time, and radio broadcasting was by contrast well

advanced, their proposals were not widely embraced. In general, any suggestions for signal searches in the optical regime were at first ruled out because of the aforementioned energy considerations.

2.2.1 The Technical Case for OSETI

However, in the last twenty years, Townes and others have continued to insist that optical signals are viable, and that SETI should be expanded beyond the radio and microwave frequencies.[1] In [34], Townes argues that for a civilization unknown to us, energy expenditure may not be the primary constraint one might consider when broadcasting signals: the simplicity of the transmission device, the possibility of signal dispersion, and availability of raw construction materials could be equally important. Nevertheless, one can make further modifications to our original assumptions that render optical signals much less unrealistic, and in fact potentially more desirable. Significantly, laser technology is still rapidly advancing, while radio transmission technology has essentially reached a stasis [23], a fact that will be discussed further below. This changes the basis from which to evaluate the probable technology of an extra-terrestrial civilization, immediately increasing the viability of an optical signal transmission.

We here present the prevalent quantitative analysis of received signal power, as derived in [5], as a means of examining the viability of optical signals. Subscripts of 'R' and 'T' represent quantities received and transmitted, respectively. First the ratio of powers is directly proportional to the ratio of the solid angle that the receiver subtends, with respect to the transmitter, and the solid angle of the signal itself, which gives us a received power equal to:

$$P_R = P_T \frac{\Omega_R}{\Omega_T}. \tag{2.1}$$

Since $\tan x \approx x$ for small x, we can substitute

$$\Omega_R = (D_R/R)^2 = A_R/R^2, \tag{2.2}$$

[1] When Townes discusses "optical" signals, both infrared and visible frequencies are implied. In the Harvard–Smithsonian-Princeton project, the telescopes are attuned only to visible frequencies.

where R is the distance from transmitter to receiver and A_R is the area of the signal detector, with D_R as its diameter. Thus with complete generality we obtain

$$P_R = P_T \left(\frac{A_R}{R^2 \Omega_T} \right). \tag{2.3}$$

The solid angle subtended by the transmitted signal is found using Rayleigh's criterion, which caps the resolving capability of a telescope (given the telescope diameter) [20]:

$$\theta = 1.22 \frac{\lambda}{d}. \tag{2.4}$$

Ignoring constants of order one, the signal's solid angle is

$$\Omega_T \approx \theta^2 \approx (\lambda / D_T)^2 \approx \lambda^2 / A_T, \tag{2.5}$$

where D_T is the diameter of the transmission device. For the diffraction-limited transmitter above, the power equation can now be written as

$$P_R = P_T \left(\frac{A_T A_R}{R^2 \lambda^2} \right), \text{ or } P_R = P_T \left(\frac{D^4}{R^2 \lambda^2} \right), \tag{2.6}$$

assuming that the diameters of the receiver and transmitter are approximately equal–not unreasonable given our assumptions regarding relative technological sophistication.

The received power is dependent on a number of factors other than transmitted power, including transmitter sizes and, less obviously, the detection technique, which can either be straightforward photon-counting or heterodyne detection. In heterodyne detection, the beam entering the telescope is multiplied by a generated signal of known frequency and amplitude, and the difference frequency signal is measured to obtain the frequency and amplitude of the incoming signal. Straight photon-counting is done with a photodiode, a photomultiplier tube, that consists of a photocathode and an anode held at a given voltage difference. A sufficiently energetic photon hits the photocathode, generating an electron via the photoelectric effect that is accelerated to the anode where the signal enters the circuitry as a pulse of a given voltage.

Heterodyne detection introduces a quantum uncertainty (amplitude and phase can

be measured, thus creating an error in both) which is proportional to the energy of the incoming photon [35]; this noise must necessarily increase for higher frequency signals. Photon-counting, on the other hand, is ideal for the detection of high frequency transmissions, especially if those transmissions come in discrete pulses, which is what we might assume anyway given the higher instantaneous transmission energy needed. From Townes' many exhaustive tables, we present Table 2.2. We note that similar S/N ratios are achievable for both detection systems, but that the $10\,m$ telescope, observing at a wavelength of $\lambda = (1/1,000)\,cm = 10\,\mu m = 10,000\,nm$, has the best S/N of all. Thus we bring the infrared and visible spectra well inside the realm of plausible transmission and detection, on the basis of the signal to noise ratio for a set transmission power [22].

$1/\lambda,\ cm^{-1}$	S/N	$1/\lambda,\ cm^{-1}$	S/N
1/30	7.8	10	8.7×10^{-2}
1/10	4.5	30	2.7×10^{-1}
1/3	2.2	100	2.6
1	1	300	5.5
3	1.4×10^{-1}	1,000	18

Table 2.2: Signal to noise ratio, presented as a function of inverse wavelength, $1/\lambda \propto \nu$, for a fixed transmission power. The left-hand columns assume a transmitter size of $100\,m$, and the use of heterodyne detection, which is appropriate to the long wavelengths. The signal to noise in the right-hand columns are calculated using a $10\,m$ transmitter and signal detection by photodiode methods [35].

2.2.2 Directed-beam Transmission

We have assumed that transmitted signals not intended for interstellar communication would be given off isotropically, thus reaching any and all life within their range. However, as mentioned above, it would greatly reduce the required power if a transmitter could target planetary systems around particular known stars [34, 5]. To get a feel for the great advantages of a directed, as opposed to isotropic, signal, we return to Eqations 2.3 and 2.6.

We would like to find the relative transmission powers needed for a given received power for the two transmission methods, and so re-create the estimates of relative transmission power that Townes gives in [34]. We assume a signal of one photon per

second striking a receiver of diameter $100\,m$ located a distance $1,000\,ly$ ($R^2 \approx 10^{38}\ m^2$) from the source. The receiver area is 10^{-35} of the area of a sphere of this radius, and thus for an isotropic transmission, a received signal of 1 photon per second implies 10^{35} photons per second leaving the transmitter, or a power of

$$P_{T_{iso}} = 10^{35} h\nu = 10^{35} \frac{hc}{\lambda} \approx \frac{2 \times 10^{10}}{\lambda}\ W, \tag{2.7}$$

for λ given in meters, where $h = 6.63 \times 10^{-34}\ J \cdot s$ and c is the speed of light. In the second case, for a directed signal, we assume that the transmitter is of equal size as the receiver. The desired power received P_R remains $\frac{2 \times 10^{-25}}{\lambda}\ W$; by Equation 2.6, with λ again in meters,

$$P_{T_{beam}} = \lambda \cdot 2 \times 10^5\ W. \tag{2.8}$$

The isotropic signal is more efficient for very long wavelengths, $\lambda^2 \geq 10^5\,m^2$. This corresponds to $\lambda \approx 3 \times 10^2\ m$, though, which is 1,500 times longer even than the $21\,cm$ emission line of hydrogen. Given Rayleigh's criterion and a transmitter of diameter $100\,m$, though, even a "directed" beam at these wavelengths would be isotropic ($\Omega \approx (\lambda / D_T)^2 \approx 9$, which is of order 4π). At shorter wavelengths, though, a directed signal is actually directed, and it is far more efficient than its isotropic counterpart: for $\lambda = 10^{-5}\ m$, the necessary power for a directed signal is only $2\,W$, or fifteen orders of magnitude less than in the isotropic case. Note also that the beam of a $100\,m$ telescope transmitting at $\lambda = 10^{-5}$ subtends an arc of about $10^{-7}\,rad$, or $10^{12}\,m$ at a distance of $1,000\,ly$. One AU, the distance from earth to our sun, is only $1.5 \times 10^{11}\,m$, so our planet would be well within the range of such a beam directed at our star.

System Parameters and Directed–beam Transmission

We have seen that a directed beam is feasible from energy considerations, but is it technically viable, and would it overcome the noise from its own star? Horowitz et al. [23] note that lasers under development at Lawrence Livermore National Laboratory are capable of short, highly energetic pulses, on the order of $10^{15}\ W$ or higher in the space of nano- or even femptoseconds. Such pulses, concentrated as they are in time, would

be easily distinguishable above the background of a sun-like star even for separation distances greater than $1,000\,ly$. As an example, consider receptor and transmitter telescopes each to be of diameter $10\,m$ (the size of the Keck telescope in Hawaii), with the transmitter located on a planet orbiting a star of apparent magnitude $m_V = 2$, one of the brightest stars our project observes.[2] As a benchmark [23], a $1\,m$ telescope located $1,000\,ly$ from a twelfth magnitude star would receive $\approx 3 \times 10^5$ photons/s; using a $10\,m$ telescope, this number increases to 3×10^7 photons/s. To determine the signal due to a second magnitude star, we invoke the relation [25]

$$I_{m_V} = I_\circ 10^{\frac{-(m_V - m_\circ)}{2.512}}, \tag{2.9}$$

with $m_\circ = 12$ and $I_\circ = 3 \times 10^7$ photons/s. Thus any transmitted signal must overcome this upper bound on the background of $I_{m_V} = 3 \times 10^{11}$ photons/sec.

In calculating the signal received by our sample laser, we first note that even at a distance of $1,000\,ly$, a $10\,m$ diffraction-limited telescope emitting a signal at $1.047\,\mu m$, the most comfortable wavelength for the laser mentioned above, produces a beam that would extend at least 1 AU in radius out from our star (see Equation 2.4). We also note that this wavelength is not in the visible spectrum; if it were, the rate we calculate below would increase by an order of magnitude. The number of photons arriving in our detector is easily deduced from Equation 2.6. With N_R as the number of photons received per unit time, $P_R = \frac{N_R hc}{\lambda}$. Thus, with an additional factor to account for photon extinction [23], and considering the transmission and detection telescopes to be circular and of equal diameters, we obtain

$$N_R = \frac{(\pi D_T D_R)^2 P_T}{16 hc \lambda R^2} 10^{-4R/5R_E}. \tag{2.10}$$

In this equation, the characteristic distance for photon extinction R_E is the radius at which a signal of $\lambda = 1\,\mu m$ decreases by two magnitudes (again, the λ of our laser is

[2]The apparent magnitude of a star is a measure of how bright it appears to be in the sky. The scale of apparent magnitudes, denoted m_V as opposed to the absolute magnitude M, was first developed by the Greek astronomer Hipparchus ca. 150 BC. The scale was refined and standardized in the nineteenth century, but it retains its original orientation: the brightest stars have the smallest magnitudes [25].

approximately $1.047\,\mu m$); R_E increases rapidly with increasing wavelength [23]. For $\lambda = 1\,\mu m$, $R_E \approx 1.15\,kpc \approx 3,700\,ly$, and the extinction factor is about 0.61. Thus we have photon arrival rate of almost 2×10^{11} photons/s, or 540 photons per $3\,ns$ interval, the pulse length of the laser cited in [23]. This rate is only comparable to the background, not appreciably greater. However, our example was just that, and there are many ways of increasing the S/N ratio without difficulty. A star with $m_V = 4$ already has a noise rate that is a tenth of the example laser pulse, the wavelength of the transmitted signal could easily be made shorter, the laser mentioned here is not the most powerful we can conceive of, etc. The point is taken that earth technology exists now that could produce a directed signal that is at least as strong as the background, and that more powerful signals are entirely reasonable.

From an energy standpoint, the desirability of directing signals at specific stellar systems rather than at the whole sky places more importance on the estimates Cocconi and Morrison first presented of the number of "interesting" stars within a reasonable distance of our sun. For if we can postulate that a signal might be directed straight at our sun, why not turn the logic around and observe only stars from which signals are likely to come? Better instrumentation and cataloging have increased the number of known potential signal sources. The 11,000 or so stars that the Harvard–Smithsonian-Princeton project intends to observe is a round number, and certainly does not represent all the stars that might be viable. The number of F and G stars alone increases by 1,000 as we move out from $100\,ly$ to $1,000\,ly$; our project observes K stars as well.[3] We therefore close our discussion of the rational and technical justification for optical SETI and turn to the specifics of the Harvard–Smithsonian-Princeton OSETI project itself.

[3]The letters F, G, and K refer to the spectral classification we assign to stars, depending on their luminosity. F stars have average luminosity of about five suns, while K stars' luminosity are about half that of the sun. Our sun is a G star [25].

Chapter 3

OSETI at Harvard–Smithsonian–Princeton

3.1 Experimental Facilities and the Benefits of Simultaneous Observation

3.1.1 OSETI at Harvard–Smithsonian

The OSETI experiment at Harvard–Smithsonian that Princeton joined in November 2001 is designed to detect signals from an energetic pulsed laser of the sort discussed in Section 2.2.2. Observations on the Harvard end are made at the Harvard/Smithsonian Oak Ridge Observatory outside of Boston using the $61\,in$ Wyeth reflecting telescope there [23, 28]. The telescope will observe more than 11,000 F, G, and K stars within $100\,pc$ ($326\,ly$) [28] looking for high-amplitude pulses on nanosecond time scales. The types of star chosen for observation are, as mentioned above, generally similar to our sun; types that vary significantly, such as M stars, are rejected on the basis of stellar stability and the size of the habitable zone for planetary orbits [28]. The OSETI project takes advantage of the observations made by another experiment being conducted simultaneously at Oak Ridge which does spectral analysis of stars that might harbor life. Making use of the light that is reflected from the aperture of the spectrograph, approximately 25-35% of the total light is directed into the OSETI apparatus for signal

detection and analysis.

Because the spectroscopy survey ultimately measures Doppler shifts in stellar radial velocities, multiple observations of each star are needed over a period of months and years: hence a collection as of November 2001 of 45,650 observations of only 7,382 stars [28]. The repetition in stellar observations is helpful to the OSETI project as well, as we can then look for potentially significant patterns in multiple observations of a given star. Almost all the selected stars have apparent brightnesses $m_V \leq 11$, making repeated observations much easier since the spectrograph does not require much exposure time.

3.1.2 OSETI at Princeton

The nightly observations at Princeton are made on the campus of the University at the recently refurbished Fitz-Randolph Observatory, which houses a $36\,in$ reflecting telescope. Both the Princeton and Harvard telescopes have Cassegrain focus: a concave primary mirror reflects the light back up onto a secondary mirror centered on the axis of the telescope which then focuses the light onto the eyepiece through a hole in the primary mirror. One difference in the Princeton observations is that virtually all of our light goes to the OSETI setup, with a small fraction used by a CCD camera to track the target star. Although plans are in effect to begin observations of and a search for comets and asteroids, there is currently no project at Princeton like Harvard's spectroscopy survey to compete with OSETI.

The Harvard–Smithsonian OSETI project made its first observations on 19 October 1998; Princeton joined in on 1 November 2001. On nights when the skies are clear in Boston and in Princeton, the two telescopes perform simultaneous observations of the stars chosen for the night by the spectroscopy project. Whenever the telescope operators at Oak Ridge change coordinates, Princeton receives an automated message which the operators at Fitz-Randolph must accept to begin observation.[1]

[1] We add one caveat: the message to change target coordinates does not always get through. After Harvard has moved its telescope to a target and we receive the coordinates, Oak Ridge may decide not to observe that target after all, but to move on. Princeton does not always get notice of the second change, and on occasion we end up not observing the same star as Harvard. In the catalogue of Princeton observations that yielded "good" hits (explained below) between 1 November 2001 and 28 February 2002, ten out of seventy stars were not observed at Oak Ridge on the same night. There is now a better, live communication line between the two telescopes which we hope will avoid these confusions.

The clocks in the circuits of each telescope detection system are set by a pulse from the same GPS source, re-synchronizing them every second. A 10 MHz oscillator runs in each circuit and the counter associated with it halts upon receipt of a coincidence signal: thus the absolute time at the two observatories should be accurate to an error of $\pm 100\,ns$ [23]. The Princeton group puts the accuracy of a coincidence measurement between the two telescopes as rather higher: 20 μs [37]. The latter is a very conservative estimate based on time delays in the circuit, including in the wires that transmit the satellite GPS signal to the computer. However, the criterion that determines simultaneity between the two telescopes is less demanding. Taking the distance between Princeton and Harvard (the baseline) to be $\approx 480\,km$, the light travel time between the two is $1.6\,ms$, providing us with a window of experimental error within which we may conclude absolute coincidence of two signals.[2] The actual error allowed by the light travel time will depend on the position of the star we are observing; $1.6\,ms$ is the maximum delay and would occur if the star were low on the horizon and collinear with the baseline.

Provided that a coincidence is ever observed within the window created by the light travel time, the benefit of the simultaneous observation is to eliminate virtually any chance that the signal would be accidental. To see the surety with which we could label relevant such a close coincidence, take, as Horowitz does in [23], the rate r_g of "good" hits to be about one per hour at each telescope. In a sampling time of $\Delta T = 1\ ms \approx 3 \times 10^{-7}\,hr$ within we would accept the signal correlation, the probability of one telescope getting a good signal is $r_g\,\Delta T = 3 \times 10^{-7}$. The probability of both telescopes getting such a hit is the $(r_g\,\Delta T)^2$, which is equal to the combined rate r_b times the sampling time. Thus $r_b = (r_g\,\Delta T)^2/\Delta T = 3 \times 10^{-7}$ hits per hour, or an average of three accidental simultaneous hits in 1,000 years of observing time—a rather low background!

[2]Though we would like to observe coincident signals at the two sites within $1\,ms$, the software that performs the preliminary data analysis currently notes any signals that fall within $3\,min$ of each other. Much of the discussion above is still theoretical given that the best candidate signals thus far were $13\,s$ apart.

3.2 Inside OSETI: Opening the Black Box

Both telescopes have an instrument, called the OSETI box, that is the basis for the entire experiment. A schematic diagram of the identical electronics used at Harvard and Princeton is given in Figure 3.1, the mechanical difference in the two setups, again,

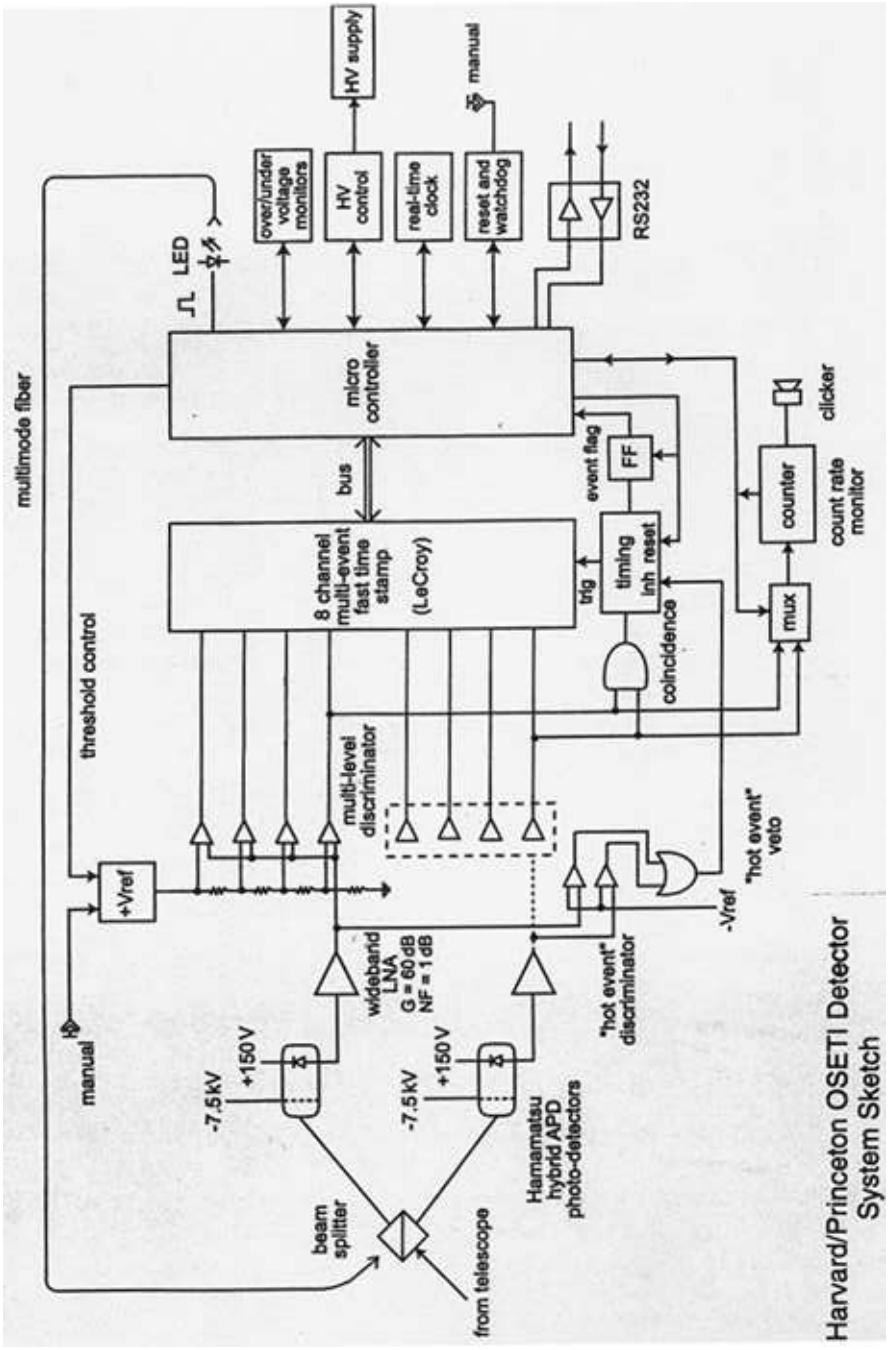

Figure 3.1: Inside the OSETI box: a schematic diagram. Light enters from the telescope and hits the beamsplitter at the left of the diagram. Figure found in [37] and at the Harvard OSETI website, http://seti.harvard.edu/oseti/pics/elecblock.gif.

being that at Princeton the light from the telescope goes directly into the box, with only 4% reflected to the CCD camera, which we use to track the star [37]. At Fitz-Randolph, this is accomplished by an aluminized mirror with a spot of clear glass in the center that allows 96% of the light from the telescope to enter the OSETI box (see Figure 3.2).

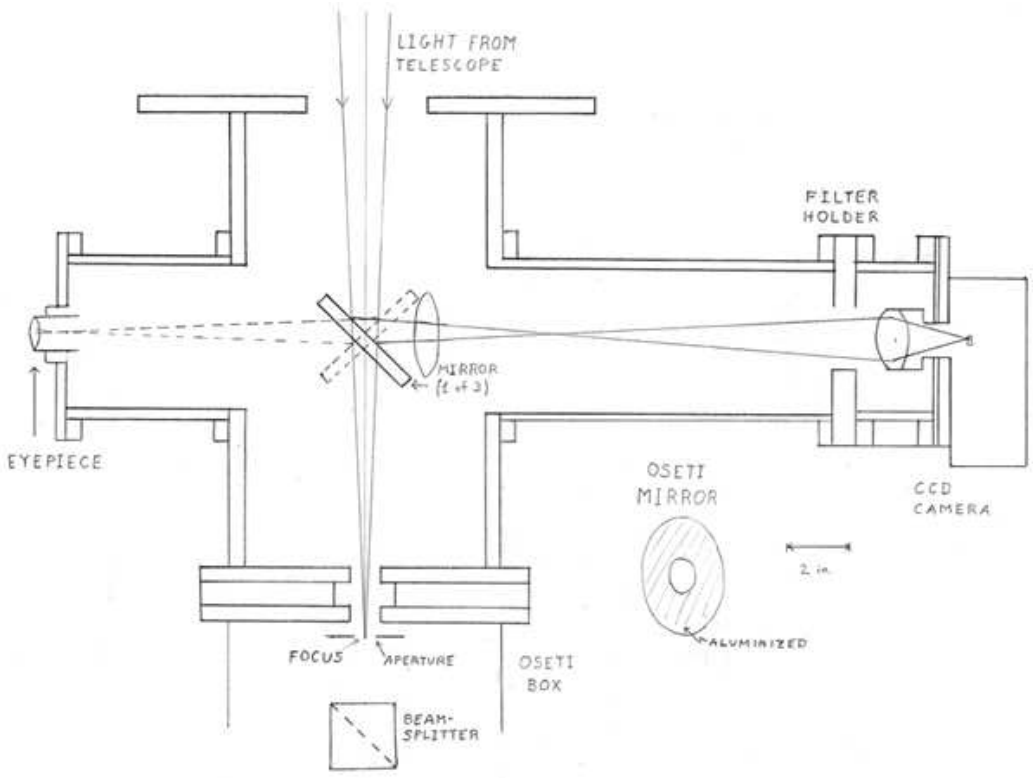

Figure 3.2: A diagram of the observer's end of the Fitz-Randolph telescope. Simply by changing the mirrors at the vertex of the diagram, the light entering from the telescope can be directed in three ways: to the eyepiece at left, to the CCD camera at right, or to the OSETI box. Diagram adapted from that of D.T. Wilkinson, 23 Aug 01 [37].

The OSETI box encapsulates the objective of the experiment: to observe and record any signals on short time scales that are brighter than the ambient starlight. The circuitry is complex largely because the timing must be so fast and so accurate and also because we do not end up looking at one signal alone, though the final product is again a

single hit, either good or bad. Just as the simultaneous observations between Princeton and Harvard reduce the overall systematic error of the system, the OSETI box performs simultaneous observations on a single signal entering the telescope by first splitting that signal in two. A half–silvered mirror directs equal portions of the incoming light to two photodetectors, which in turn convert the incident photons into photoelectrons. In the process of converting the photons to a voltage signal and then amplifying that, there are possibilities that random electron cascades in the photodiodes would mimic a bright pulse from the telescope itself. By dividing up the light we are actually interested in, we leave unchanged any information in the incident light while greatly decreasing the background of spurious hits generated by the circuitry.

The photodiodes that produce the voltage signal have an efficiency of approximately 10%; that is, one of ten incident photons will produce a photoelectron. The electron is accelerated through a potential difference of about $8\,kV$, after which it hits an internal diode causing an avalanche with a gain of 70,000 for our $150\,V$ bias voltage [21]. The resulting signal is further amplified before entering the main part of the circuit. The signal voltage from each channel is then compared to four levels of reference voltage. The particular photodetectors that the circuits use give very good pulse height resolution, meaning essentially that the signal amplitude will be directly proportional to the number of photoelectrons that hit the diode at the same time (see Figure 3.3). In Harvard's circuitry, the four voltage levels are set to correspond to the arrival of 3, 6, 12, or 24 ($3 \times 2^{0,1,2,\,or\,3}$) photoelectrons [23], whereas at Princeton the levels are lower, corresponding to 2, 4, 8, or 16 photoelectrons. Figure 3.3 shows what appears on the oscilloscope screen when brief optical signals, like the ones we intend to observe, are sent in; the pulse height changes linearly and dramatically with the number of input photoelectrons. We see also that the pulses are not, of course, instantaneous, and the existence of finitely sloped leading and falling edges allows us to record the basic shape of each pulse. A very fast timer made by LeCroy (MTD135[3]) outputs a number, corresponding to time, whenever one of the four voltage thresholds is crossed by the incoming pulse, both rising and falling: these interval numbers are the primary data output (see Section 3.3.1 for

[3]The LeCroy timer used in the OSETI boxes at Oak Ridge and Princeton is a Multi-hit Time-to-Digital converter, model MTD135, capable of recording up to sixteen hits on each of eight channels [29].

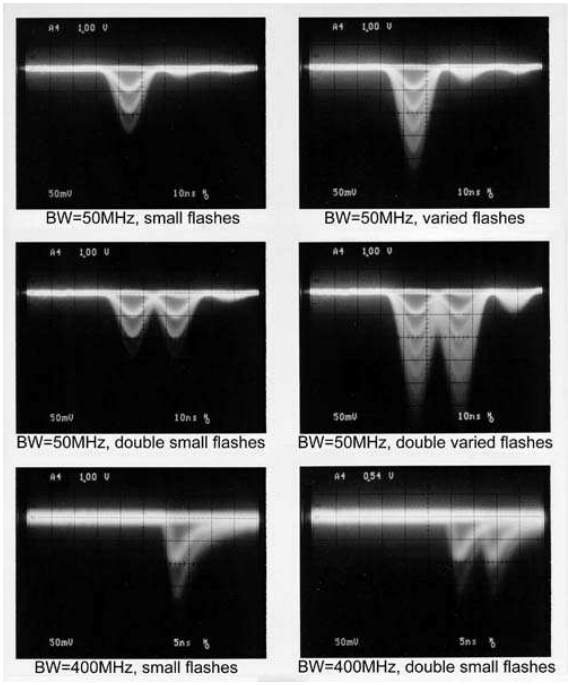

Figure 3.3: Oscilloscope photographs of what the OSETI detector sees when a short flash of light is sent through the circuit. The electrical pulses are negative (so you don't confuse them with mountains); the top four pulses are only about $10\,ns$ long, while the lower two pulses show the detector's capability to resolve on time scales of $5\,ns$. The pulse–height resolution of the photodiodes is impressive; the incidence of pulses of one, two, three, etc. photoelectrons appear as increasingly deeper bumps. Photos found at the Harvard OSETI website, http://seti.harvard.edu/oseti/photos.htm#flashes.

further details).

Before the circuit starts recording the nature of the pulse, we first make sure that both photodiodes and the thresholds they lead to ("channels," as we shall now call them) have fired. From now on we will use the term "coincidence" to describe a simultaneity across Channels A and B; this should not be confused with coincidences between the Princeton and Harvard telescopes, which we will not discuss further. The part of the circuit labeled "hot event discriminator" is designed to immediately remove from consideration any signals of very high voltage that propagate through either or both of the channels.[4] Any signal that is not vetoed by the hot event discriminator we will

[4]We assume that such a high voltage signal would be the result of arcing in the electronics and

henceforth call a "hit." Hits are recorded as follows: as soon as any signal propagates through either channel, regardless of coincidence, the MTD automatically records the rise and fall times for each threshold. Meanwhile, if there is a coincidence, signals from each of the lowest voltage thresholds combined to power a circuit that begins to charge a capacitor. It takes about $94\,ns$ for the capacitor to charge to half its maximum voltage; if the capacitor gets that far, the circuit beyond the capacitor is triggered and a signal is sent to the MTD to record a hit.

However, before the signals from channels A and B even reach the voltage thresholds, the veto circuit evaluates whether or not the pulses in the channels constitute a positive coincidence, or hit. The hot event veto has $94\,ns$, while the capacitor is charging, to detect a bad signal. If it does so, the circuit charging the capacitor is reset. Since the capacitor does not charge sufficiently, no coincidence signal is sent to the MTD, which discards whatever data it had collected [14]. In the next section, we will look more closely at the timing of the MTD and how exactly to interpret the data that results.

The final components of the circuit, dominated by the microcontroller, have to do with the auxiliary data-taking in the system: recording the timestamps seen by the MTD, keeping track of the total number of coincidences, and performing diagnostic tests at the start of each new stellar observation. Among the most important of the tests, other than those simply determining that each circuit element is alive and responding, is the simulation of a photon event via an LED flash into the beam splitter. Provided the high voltage sources for the photodetectors and the discriminator levels are on (both are checked in the second stage of the diagnostic tests), the LED flash should be read by the OSETI circuit: if it is, we can be very sure that the entire system is functioning [13].

3.3 Reading the Data

To elucidate the discussion above and provide a reference for the coming data analysis, we present in Figure 3.4 an example of the way the data ultimately appears in the

thus not a viable extra-terrestrial signal. However, by inserting an "OR" gate rather than an "XOR" (exclusive OR) gate, we remove our capability of observing pulses of very high energy. *Revised 27 May 2002.*

Observation 1008

```
System diagnostics started at 2002-02-09 02:40:17.26-05
 Low threshhold count rate channel A (100 ms): 0.09
 Low threshhold count rate channel A (200 ms): 0.055
 Low threshhold count rate channel B (100 ms): 0.23
 Low threshhold count rate channel B (200 ms): 0.205
High threshhold count rate channel A (100 ms): 0.01
High threshhold count rate channel A (200 ms): 0.01
High threshhold count rate channel B (100 ms): 0.01
High threshhold count rate channel B (200 ms): 0.01
Object:  HIP069311
V magnitude:
Observer:
Temperature:
Clouds:
Integration start: 2002-02-09 02:40:22.92-05
Integration stop: 2002-02-09 03:01:10.43-05


Coincidence number: 6848
Date/time: 2002-02-09 02:59:26.60-05
Timestamp: 5859284
Quality: Bad
A(rise) A(fall) B(rise) B(fall)
-1      -1      -1      -1
-1      -1      -1      -1
420     409     -1      -1
420     409     430     -1

Coincidence number: 6847
Date/time: 2002-02-09 02:50:17.18-05
Timestamp: 1474153
Quality: Good
A(rise) A(fall) B(rise) B(fall)
-1      -1      -1      -1
-1      -1      -1      -1
430     417     -1      -1
430     417     430     418
```

Figure 3.4: Our sample data: an entry in the the Princeton OSETI log file showing two coincidences from the star HIP069311, $m_V = 10.2$, observed on the night of 8 Feb 02. This section comprises the discussion on how to read the log file.

OSETI log files at each telescope's computers. The first lines, beginning with "System diagnostics started at [Date/Time]" and ending with "Integration stop," constitute the header information of each observation in the log file. Only if the system passes the preliminary diagnostic tests mentioned above does the real data-taking begin, indicated by the printing of the header to the log file. The header identifies three times: the time the diagnostics were started and the integration start and stop times (that is, the times between which the system actually made observations of a given star). Dates and times are always given in order of increasing specificity: year, month, date, hour, minute, second, hundredth of a second. Times are recorded relative to the local time zone, indi-

cated by the *-05* that qualifies every Date/Time line: Princeton and Harvard are both five hours behind universal time measured at the Greenwich meridian. Note that the system diagnostics take approximately five seconds to run before the integration starts; an identical discrepancy occasionally surfaces in the database, depending on whether or not the time observed is mistakenly calculated from the start of the diagnostics.

In addition to the observation times, the header is intended to provide basic information about the star and the observing conditions. The "Object" line indicates the star name; Figure 3.4 shows one classified by its number in the Hipparchos catalogue, HIP069311. In the log files of the Oak Ridge telescope, the next four lines are not blank, as they are in the Princeton files, and their contents are specific to the weather at Oak Ridge and whichever member of the spectroscopy project is on duty that night. In general, the absence of this information is not a hardship, and since Observation 1008 was recorded, the V magnitude has been included in the Princeton log file as well.

Lines two through nine in the header require more explanation, and in fact result from the last stage of the diagnostic tests. After ensuring via the LED flash that the OSETI box is live, the box looks briefly at the star itself and records what channels A and B observe, independent of one another, for all permutations of two parameters (hence the eight lines). For the given channel, the "Low threshold" count rate gives, in kilo-photoelectrons per second (kpps), the number of times the lowest energy threshold is crossed during two time intervals. The lowest energy level is set to reflect the arrival of single photons, so it should be related to the expected number of photons arriving from a star of given magnitude (cf. Equation 2.9) after accounting for the conversion efficiency and any other possible signal attenuations before the light hits the photocathode. The dependence of the kpps rates on star magnitude will be further discussed in Section 4.2 in the analysis of the data. For now, we note that HIP069311 has a V magnitude of 10.2, making it one of the dimmer stars that we observe and giving our sample observation rather low kpps rates overall.

We observe for two time intervals primarily as an internal system check; the rates for the $100\,ms$ and $200\,ms$ intervals should be approximately equal. In Observation 1008, the $100\,ms$ number for the low threshold rate of Channel A is 0.09, indicating

90 photoelectron events per second observed by the system. The same rate for $200\,ms$ is lower, only 55 photoelectron events per second, but still within the same order of magnitude. The low threshold numbers for the two time intervals on Channel B are even closer: 230 and 205 photoelectron events per second for the shorter and longer intervals respectively. The high threshold rates reflect the arrival of multiple photoelectrons simultaneously; hence by probability arguments we would expect them to be much lower than the low threshold rates, as they are. Internally, at least, the channels' kpps numbers seem to be consistent with our expectations. However, the significant difference in the kpps rates of the two channels is indicative of an imbalance in the two branches of the circuitry, for which there is more evidence in the data itself (see Section 4.2).

3.3.1 Positive Coincidences (Hits) and Timing

Having finally disposed of the header information, we move on to the actual hits. Each entry for a hit records first its number in the running total maintained by the counter shown at the bottom of Figure 3.1.[5] Next on record is the first order system time given to $0.01\,s$ by the GPS. The seven digit "timestamp" on the next line improves that accuracy to an error of only $100\,ns$, as mentioned earlier. It is the number at which the 10 MHz counter stopped upon receiving a signal of a positive coincidence, and if necessary it is padded with zeros at the front so as to be always seven digits [17]. The first number in the timestamp is the tenth of a second, so the more accurate version of the time for coincidence number 6848 would be not 02:59:26.60, but rather 02:59:26.5859284. The GPS clock runs slightly ahead of the timestamp, so it is possible for the clock to show a change in the second when the timestamp records an event late in the previous second. For example, a timestamp of 9876543 with a time of 00:00:01.03 would actually represent a time of 00:00:00.9876543.

Our particular model of MTD is purportedly capable of counting as rapidly as once every $500\,ps$ (or $0.5\,ns$), but in reality, it is a bit slower, moving one increment every $0.625\,ns$. The MTD, like the 10 MHz oscillator that gives us our timestamp, simply

[5] Unfortunately for our convention defined in Section 3.2 the data log labels hits as coincidences. Do not be confused: the only events that make it into the log are coincidences that were not vetoed by the hot event discriminator, that is, positive coincidences, or hits.

records the number of cycles it passes through, which we then interpret as the passage of a certain amount of time. Thus to the rise and fall events, the MTD assigns numbers corresponding to the number of $0.625\,ns$ intervals that have gone by. To link these increments explicitly to the timestamp in the event of a hit, the same signal of a positive coincidence that triggers the MTD also triggers the timestamp. From the timestamp and the rise and fall numbers we can then calculate the rise and fall times of the signal to the tenth of a nanosecond, a process discussed in greater detail at the end of this section.

As we mentioned earlier (cf. Section 3.2), the MTD records whatever signals it receives, and only after a delay does it receive the notice to retain the data gathered on a positive coincidence. It follows, then, that we have to work backwards to obtain the actual rise and fall times of the incoming pulse, which are then recorded in the four columns labeled "A/B(rise/fall)." The way the data is arranged in the log file is already a schematic diagram of sorts; each of the four rows represents one of the four energy thresholds against which the circuit compares the signal. The default output value of each threshold for both rise and fall times is negative; as one can see, the highest levels in each of the two pulses in Figure 3.4 are all -1, indicating that the pulse was not energetic enough (that is, it did not contain enough photons) to reach those levels. If the pulse crosses a threshold, the log file records a nonnegative number that tells us *when* it did so. We expect pulses similar in shape to the ones shown in Figure 3.3, so one pulse should cross a given threshold exactly twice; these are the rise and fall times. To further clarify, we include a schematic pulse diagram in Figure 3.5, exactly of the sort that one can reconstruct from the log file. To emphasize how the system works, this imaginary pulse is much broader than the pulses we actually observe; its width, as measured between the crossings of the lowest threshold, would be $(440 - 380)0.625\,ns/\text{increment} \approx 38\,ns$. We see from Figure 3.4, coincidence number 6847, that the pulse in channel A rose and fell almost instantaneously, and lasted only about $(430 - 417)0.625 \approx 8\,ns$, with a similar duration for the pulse in channel B.

As they appear in the log file, these numbers are not times, but rather increments of the MTD. If a pulse is not vetoed by the hot event circuit, the capacitor discussed in

Threshold							
4							
3			R	F			
2		R			F		
1	R						F
Time →	440	430	420	410	400	390	380

Figure 3.5: A "picture" of the pulse itself, as it propagates through one channel, obtained simply by recording the time at which each voltage threshold is crossed. The direction of time on the horizontal axis is correct, but the numbers are the increments produced by the MTD, as discussed in 3.3.1. The times for the "R" would be recorded in the data column "A(rise)," while the "F" would be listed under "A(fall)." As in the log file, the top row of columns here corresponds to the highest energy threshold [11].

Section 3.2 charges in the $94\,ns$ allowed it and sends off the message that there has been a hit. This message, too, is retarded. After going through a number of logic gates and another built-in delay, it reaches the MTD after about $225\,ns$ from the initial arrival of the pulse, as calculated by C. Coldwell in [14] (the $225\,ns$ includes the $94\,ns$ interval allowed to the hot event veto). The added delay ensures that the signal of a positive coincidence will arrive long after the MTD input circuits have settled; after all we are expecting pulses that last as briefly as $10\,ns$.

The numbers that are displayed in the final data readout represent the number of increments between various traces of the pulse, recorded by the MTD, and the arrival of the coincidence signal. This explains why the numbers in the "rise" columns are greater than those in the "fall" columns: the rise times represent earlier events, and thus a larger difference in MTD increments. In coincidence number 6847, for example, in Figure 3.4, Channel A rose $(430)0.625\,ns/\text{increment} = 268.8\,ns$ *before* the timestamp of $0.1474153\,s$, and Channel A fell $(417)0.625 = 260.6\,ns$ *before* the timestamp. Thus the length of the pulse was approximately $8.2\,ns$, and the leading edge actually crossed the first threshold at $0.147415031\,s$. The single, unavoidable path that the coincidence signal must follow to reach the MTD implies that the rise and fall numbers will be nearly identical for every coincidence: the circuitry doesn't change. As a sanity check, we note that a low estimate of $225\,ns$ for the coincidence signal to reach the MTD would yield outputs in the neighborhood of $225/0.625 = 360$ increments: almost all the coincidences

examined by the author contain numbers in the low 400s.

3.3.2 First Order Data Analysis

In the preceding discussion of the record of coincidences that gets written in the log file, we skipped the line labeled "Quality." Now that we know what the numbers in the rise and fall columns mean, we return to the label, good or bad, assigned to each coincidence.

Software written by Charles Coldwell of the Harvard OSETI group performs the main analysis of the coincidences recorded by both telescopes. Even when the hot event veto does not act, the software weeds out most of the more bizarre signals that are inevitably recorded. The program implements in code the first six of the seven criteria listed below [11]:

1. At least one threshold on both channels must be exceeded.
2. The maximum threshold crossed on one channel must be within ± 1 level of the maximum threshold crossed on the other channel.
3. The maximum rise threshold must be the same as the maximum fall threshold on each channel independently.
4. Rise times must get later as thresholds increase on each channel independently (though this means that the numbers shown will actually decrease).
5. Fall times must get later as thresholds decrease on each channel independently (again, the numbers will decrease).
6. Fall times must be later than rise times.
7. An entry of zero is automatically invalid.

As a result of the author's investigations, the Harvard and Princeton groups agree that the last criterion should be included; however, as of this writing it has not been added to the code.

From our discussion above of the coincidence readout and what the rise and fall times of each channel represent, the implications of these criteria should be fairly clear. The software really just provides a common-sense check. The very first criterion automatically eliminates any non-coincidences that have slipped past the veto, while the

second ensures that the signals observed by the two channels are similar to one another (else we must suspect that they didn't have the same origin before hitting the beamsplitter). The third takes advantage of the fact that what comes up should come down if it is what we are looking for. We also make sure that whatever signals the MTD recorded are advancing in time as they should, and that the trailing edge is not somehow leading the leading edge. Finally, the stipulation against zeros arises from the origin of the numbers themselves. We are not likely to have a pulse that lasts the entire $225\,ns$ or longer, which would be implied if there were zero difference between the fall threshold crossing and the arrival of the coincidence signal. In fact, a very long signal would thwart criterion 3, as the signal might not descend within the delay allowed to the MTD; we have to accept that risk.

To return to the sample data given in Figure 3.4, we can now see why the first coincidence was labeled bad and the second one good. Though Channel A is fine here, the maximum rise and fall thresholds of channel B of the first coincidence are not identical; moreover, the fall time is nonsense. This is not the case in the second of the two coincidences, where channel A is again nicely behaved and channel B rises and falls obediently around the lowest threshold. Further, A does not rise above the second threshold, putting it within one level of B. Note also that the fall numbers are all smaller than the rise numbers, signifying that they occurred later. In evaluating criteria numbers 4, 5, and 6, the program looks only for an *increase* in the numbers, or a decrease in time, as the thresholds rise and fall: zero change, say from 430 to 430, which implies very steep slopes on the rising and falling edges, is acceptable.

Having provided, we trust, a thorough explanation of how the OSETI experiment at Harvard–Smithsonian–Princeton functions and the nature of the data we gather, we turn now to the data themselves and present the preliminary results of the first four months of data-taking at Princeton's Fitz-Randolph facility.

Chapter 4

Results and Analysis

To alleviate any latent tension that the reader may yet be experiencing, we haven't found anything so far. That is, none of the coincidences thus far indicate anything but a natural origin for the signals. However, it has proven to be extremely enlightening to look at the numbers that we have been seeing, both to understand them better and as a sanity check on the electronics and the software. We present these results and our theories regarding them in this chapter.

As stated, the Fitz-Randolph telescope began taking data on the night of 1 November 2001. Observations proceeded nightly, weather permitting, through the middle of February, when both Princeton and Harvard went off-line for a time: the Fitz-Randolph dome was not functioning properly, while the Oak Ridge Observatory was taken over briefly by another experiment. After observing on the night of 16 February, the experiment didn't resume until the night of 4 March, making the end of February a convenient place to draw the line for the primary data included in this paper. Unless otherwise stated, the data discussed is that taken by the Fitz-Randolph telescope at Princeton.

4.1 What Makes Bad Hits Bad

As discussed in Section 3.3.2, hits that are approved by the electronics are re-evaluated under more stringent criteria that throw out the vast majority of coincidences. In reality the situation is more complex even than that. In our examination of the records of hits,

Night of [Date] dd-mm-yy	Obs. No.	No. Hits total	No. Hits "good"	No. Hits: "weird"	Criterion 1 A	Criterion 1 B	Criterion 2 A	Criterion 2 B	Criterion 3 A	Criterion 3 B	Criterion 4 A	Criterion 4 B	Criterion 5 A	Criterion 5 B	Criterion 6 A	Criterion 6 B
13-11-01	73	27	1	3	2	0	11	0	3	8	6	18	5	6	0	0
14-11-01	76	21	0	0	4	0	13	1	0	0	4	18	2	7	0	5
18-11-01	136	31	2	13	0	0	11	0	3	4	10	22	3	15	1	8
21-11-01	159	10	0	0	1	0	4	1	2	0	4	7	2	4	1	5
26-11-01	190	21	1	0	2	0	7	0	1	2	8	7	6	6	0	0
01-12-01	203	32	1	1	3	0	10	0	2	8	2	17	5	18	0	4
09-12-01	307	20	0	0	0	0	12	0	2	9	3	20	2	3	0	4
27-12-01	523	15	0	0	1	0	6	0	2	6	2	13	3	3	0	8
13-01-01	719	11	0	11	0	0	3	0	0	9	1	11	2	0	0	0
25-01-01	807	33	0	33	3	0	16	0	2	16	8	33	3	6	0	10
TOTALS:		211	5	62	16	0	93	2	17	62	48	166	33	68	2	44

Table 4.1: The table above classifies what caused hits to be bad for observations made on ten randomly selected nights. Recall that the criteria incorporated in the software at the time were: 1. At least one threshold on both channels must be exceeded. 2. The maximum threshold crossed on one channel must be within ± 1 level of the maximum threshold crossed on the other channel. (Note: in the table, we label the channel with the lower threshold crossing as having failed Criterion 2.) 3. The maximum rise threshold must be the same as the maximum fall threshold on each channel independently. 4. Rise times must get later as thresholds increase on each channel independently. 5. Fall times must get later as thresholds decrease on each channel independently. 6. Fall times must be later than rise times.

there are many that are very close to being good, but perhaps show a time regression of one interval, or less than a nanosecond, and are thus discarded. Some hits have been labeled good that contained a zero in the fall time of the lowest threshold, which fits the criteria but is probably not legitimate (hence the rationale for adding a seventh criterion, mentioned above, for good hits). Further, it is debatable whether or not these points really ought to be included in the catalogue of good hits, or at least that of events to consider when looking for simultaneous hits at Harvard. Perhaps the criterion could be made slightly less stringent, requiring the progression of rise and fall times to differ from one another by not less than one or two intervals. Given the exactness with which the electrical circuits must operate—they are unusually fast—it is not unreasonable that the electronics themselves could have created some slight irregularity in recording the signal and that the pulse was really valid.

All this leads us to the data itself and some interesting revelations therefrom about the circuits themselves, particularly the apparent imbalances between Channels A and B. Table 4.1 documents what went wrong for ten observations notable for their large number of total hits, but otherwise chosen at random, and is organized according to the first six criteria for good hits given in Section 3.3.2. Our motivation was to see if there are any noticeable trends in the bad hits, and indeed there are. Despite their supposed equivalence, Channel B is far more likely than Channel A to be the source of a "bad" classification, for Criteria 3–6, while Channel A was the obvious culprit when Criteria 1 and 2 were not met. Further, in these ten observations, all but one of the "weird" hits (a classification coined by the author, signifying either a zero or an abnormally large number as one of the rise or fall times) came from Channel B; the only exception was the lone weird hit in Obs. 203.

4.1.1 Voltage Imbalances

From these 206 bad hits, is it possible to deduce where in the electronics the main problems lie?[1] From the fact that Criterion 1 is almost always violated by Channel A, we may infer that there are imbalances in the voltage settings of the threshold

[1] It may be helpful in the following discussion to refer to Figure 3.1 in Chapter 3.

levels, despite our attempts to make them equal. In other observations not included in Table 4.1, we note that there are times when Channel B does not fire at all, but they are few and much farther between than the same occurrences in Channel A. The possibility of a voltage imbalance is borne out by the similar dominance of Channel A in failing Criterion 2. (For Criterion 2, failure was assigned to the channel whose highest threshold was lower; thus if B reached the fourth threshold and A rose only to the second, as was often the case, we called it a failure in Channel A.)

There are two likely sources for a voltage imbalance that might cause the disparities we see in Criteria 1 and 2. The first is that the signal amplifiers that increase the voltage out of the photodetectors are not well matched in gain. The second possibility is that the reference voltages for the energy thresholds themselves are not equivalent between for Channels A and B. If the thresholds on B were effectively lower, a signal, even if it were equally divided and amplified along A and B, would surpass a much higher threshold on B than on A, leading to a potential failure of Criterion 2.

In general, one wonders how an event that fails Criterion 1 could ever be considered a hit. If the amplifiers, the reference voltage (in the veto), and the threshold reference voltage were all ill-matched compared with one another, one finds a possible explanation. Specifically, if the hot event reference voltage were too high, an event might not be vetoed and yet fail to surpass the first threshold on both channels.[2] Such a triple imbalance would also be consistent with the two proposals mentioned above.

4.1.2 Inaccuracies in Timing

Differences in the voltage levels are unlikely to cause the imbalances we see in Criteria 3–6 or the "weird" hits, however. These are all related to timing alone, except for Criterion 3. But even for this last, were the underlying fault not in the timing, there ought not to be a problem. What goes up must come down, after all, and if a signal were energetic enough to cross one threshold, it shouldn't have a problem crossing the same threshold a few nanoseconds later. When we posit a glitch in how accurate the circuit records the pulse rise and fall times, we re-emphasize that such a glitch would

[2] *Revised 27 May 2002.*

lie in MTD135 itself, governed by the 200 MHz external clock, and not in the 10 MHz oscillator that provides the time stamp. This reminder is useful because the coincidence data were not marked consistently with reasonable timestamps until 18 January 2002. The criteria deal with the intervals marked by the MTD, however, and it is these that go awry. As mentioned in Section 4.1, the errors that turn a hit from good to bad are often by no more than $0.625\,ns$, which could indicate nothing more than a very slight jitter in one of the data acquisition channels of the MTD.

On other occasions, most notably when weird hits occur, the counter for one channel seems to get stuck, as it were, on an abnormally large value. Of the 62 hits labeled weird in Table 4.1, 58 contain such large numbers, and 54 of those involved the rise time of the highest threshold of Channel B. Of the remaining eight weird hits, two were large numbers in the fall time of the highest level of B, only two resulted from large numbers in any level of Channel A, and the remaining four were all due to zeros in the fall time of the lowest threshold of A. The MTD can remain stuck through more than one observation, though this was only observed to be the case for weird hits in Channel B. For example, the eleven bad—out of eleven total—hits in Obs. 719 all contained the number 34453 in the rise time of the highest level of Channel B, a defect without which four of the hits would have been labeled good. Further, that same number in the same place occurs in all nine of the hits of Obs. 718, seven of the eight hits of Obs. 720, and all three of the hits of Obs. 721. Observations 717 and 722 are free of the glitch. The observations immediately before and after Obs. 136 and 807 contained no weird hits. In fact, Obs. 136 succumbed to a rise time in Channel B of 57652 only after three coincidences but righted itself again eighteen coincidences from the end of its integration time.

A puzzling feature of this already odd behavior is the one hit of Obs. 720 that didn't have the 34453: as coincidence number 3082, it was the first of the hits on that observation, yet the system does not seem to have been shocked back to normalcy, for the tell-tale 34453 reappears in coincidence number 3083. Observations 718 through 721 were made over the course of nearly an hour, a huge time scale relative to the $0.625\,ns$ timing capability of the MTD, and the other strings of weird hits took place over time

scales that were just as large relative to nanoseconds, though not as dramatic as the string from Obs. 718–721 (about five minutes for Obs. 136 and just under a minute and a half for Obs. 807).

The anomalies in timing between the two channels and the predilection of each for a particular type of error should now be clear. Though each has its problems, Channel B still has the lead in timing mishaps, weird hits aside. This is evident from Table 4.1: even if we discount Criteria 3 and 4, which are directly affected by weird hits in the top level of Channel B, there is still in Channel B a greater tendency toward illogical rise and fall times than in Channel A. The data in the table span a period of more than two months of observations and comprehend a range of star magnitudes, from Obs. 73, MIRA, which has $m_V = 2$, to Obs. 719 of 16895B, whose m_V is only 9.9 (recall that a larger m_V indicates a dimmer star). Thus it is legitimate to conclude that the anomalies we see are systematic and internal to the instrument. Further, based on the overwhelming source in Channel B of the weird hits and the timing errors they imply, we infer that B is probably the hyperactive channel, rather than A being inert.

4.1.3 Bad Hits at Harvard–Smithsonian

That the disparities we see are due to the experimental setup at Princeton is further borne out by examining the Harvard–Smithsonian data in a similar manner; the results are summarized in Table 4.2. One notices first that there are far fewer hits overall in the Harvard data set. This is not because the data was so chosen. Rather, it is a function of the events on the whole: Harvard has hit rates, both good and total, that are far lower than Princeton's, even from the same star on the same night for the same amount of time. The great disparity between the two data collection sites is worth some thought, and more quantitative discussion will be given in Section 4.3. In the meantime, suffice it to say that in an effort to even approach the number of hits analyzed in Table 4.1 the author looked at far more observations from Harvard's data than from Princeton.

From that still very limited set, we seem to see a trend similar to that at Princeton for Criteria 1 and 2: Channel A is more likely not to fire at all, or to fire less readily. However, where the MTD's fast timing circuit is concerned, there is much less disparity

Night of [Date] dd-mm-yy	Obs. No.	No. Hits total	No. Hits "good"	No. Hits: "weird"	Criterion 1 A	Criterion 1 B	Criterion 2 A	Criterion 2 B	Criterion 3 A	Criterion 3 B	Criterion 4 A	Criterion 4 B	Criterion 5 A	Criterion 5 B	Criterion 6 A	Criterion 6 B
03-11-01	22766	1	0	0	1	0	1	0	–	–	–	–	–	–	–	–
03-11-01	22773	2	1	0	–	–	–	–	–	–	0	1	–	–	0	1
03-11-01	22788	2	1	0	1	0	1	0	–	–	–	–	–	–	–	–
18-11-01	23144	1	0	0	–	–	1	0	–	–	0	1	–	–	0	1
18-11-01	23146	1	0	0	–	–	1	0	–	–	0	1	–	–	0	1
18-11-01	23166	1	0	0	–	–	–	–	0	1	–	–	–	–	0	1
18-11-01	23168	2	1	0	–	–	–	–	1	0	1	0	–	–	–	–
22-11-01	23308	1	0	0	1	0	1	0	–	–	–	–	–	–	–	–
02-12-01	23429	1	0	0	1	0	1	0	–	–	–	–	–	–	–	–
02-12-01	23430	1	0	0	–	–	1	0	–	–	–	–	–	–	–	–
02-12-01	23442	1	0	0	–	–	1	0	–	–	0	1	–	–	0	1
02-12-01	23444	1	0	0	1	0	1	0	–	–	–	–	–	–	–	–
02-12-01	23463	1	0	0	1	0	1	0	–	–	0	1	–	–	0	1
29-12-01	24010	1	0	0	–	–	1	0	–	–	–	–	–	–	–	–
29-12-01	24021	1	0	0	–	–	0	1	–	–	1	0	1	0	–	–
29-12-01	24029	1	0	0	–	–	1	0	–	–	–	–	–	–	–	–
03-01-02	24244	1	0	0	0	1	0	1	–	–	1	0	–	–	–	–
03-01-02	24246	1	0	0	–	–	–	–	–	–	0	1	–	–	–	–
03-01-02	24261	1	0	0	–	–	0	1	–	–	1	0	–	–	–	–
25-01-02	24556	1	0	0	1	0	1	0	–	–	0	1	–	–	–	–
25-01-02	24572	1	0	0	–	–	–	–	–	–	1	1	–	–	–	–
28-01-02	24633	2	0	0	–	–	2	0	–	–	0	1	0	1	–	–
28-01-02	24636	1	0	0	–	–	–	–	1	0	1	0	–	–	–	–
28-01-02	24642	1	0	0	1	1	–	–	–	–	–	–	–	–	–	–
28-01-02	24652	1	0	0	–	–	–	–	1	0	–	–	–	–	1	0
TOTALS:		29	3	0	8	2	15	3	3	1	6	9	1	1	1	6

Table 4.2: The classifications for bad hits for a more or less random sampling of Harvard's data during the same period as the Princeton data given in Table 4.1. Criteria in which neither channel failed are marked with a "–" rather than a zero.

between the two channels, at least none that could be considered statistically significant in our data set. Certainly there is nothing like the predominance of Channel B that we saw in Princeton's data, where B failed overwhelmingly in Criteria 3–6. In particular, we note in Harvard's data the relative lack of bad hits brought about by errors in the fall times of either channel (Criterion 5), and we note the relative equivalence between A and B of bad hits due to errors in the rise times (Criterion 4) in Table 4.2. These two observations taken together indicate that the MTD in Harvard's OSETI box times all eight threshold levels of Channels A and B with approximately the same accuracy.

It is likely that the MTD at Harvard is better tuned overall to its desired level of precision than at Princeton, with the following rationale: The rising edge of the pulses is steeper than the falling edge, and as the good hit criteria demand, the rise and fall times must always get later. If the leading edge crosses more than one level virtually simultaneously, it is more likely that one rise time will be an interval ahead or behind its counterparts, leading to a failure of that criterion. If the pulse falls more slowly, however, it is more likely that the time difference between, say, levels three and one will be more than a nanosecond, leaving some room for a bit of error in the time recorded for crossing level two. Given the pulses we see in the oscilloscope, we would expect more bad hits caused by Criterion 4 than 5, and indeed Table 4.2 shows this more clearly than does the Princeton data: in the former, the ratio of failures of Criterion 4 to failure of 5 is 15:2, while in the latter it is closer to 2:1. Based on a cursory comparison with Harvard's data, we again conclude that there are intermittent timing problems in the high-precision MTD in Princeton's OSETI box.

4.2 Idiosyncrasies in the KPPS Rate

Further interesting features of the Princeton coincidence data lie not in the coincidences themselves but in the kilo-photoelectrons per second (kpps) count rates for Channels A and B that are measured by the diagnostic circuit at the start of each new observation (see Table 4.3 and Section 3.3). If we look at the ratio of the kpps numbers for Channel A to Channel B, and if we accept that the average of the 200 ms low threshold ratio should

KPPS RATIOS, CHANNEL A/CHANNEL B

Obs. No.	m_V	Low Threshold		High Threshold	
		$100\,ms$	$200\,ms$	$100\,ms$	$200\,ms$
76		0.700	0.732	1.103	1.132
73	2	0.767	6.506	0.888	1.063
203	3.3	0.737	7.098	1.169	0.917
807	3.3	0.720	0.243	1.156	0.960
136	4.4	0.690	0.590	1.032	1.022
190	4.4	0.849	0.949	0.992	0.996
523	4.9	0.789	0.762	0.786	1.115
307	5	0.735	0.666	1.101	0.993
159	5.7	1.520	0.918	0.630	1.118
719	9.9	0.806	0.834	1.057	1.102
Arithmetic Mean:		0.831	[1.929] 0.712	0.991	1.042

Table 4.3: Kpps ratios for the ten observations analyzed in Table 4.1, with the average ratios given in the bottom line. Data are ordered by star magnitude, m_V. Note: The star magnitude is unavailable for observation number 76. Harvard did not observe that object, and the author has been unable to trace it by its name, *000881, as given in the log.

be closer to 0.712 than the straightforward mean inclusive of all ten observations,[3] we then see that the conclusions we drew earlier regarding a probable voltage imbalance between A and B are substantiated. That the low threshold ratios are significantly less than one implies an inherent imbalance in how receptive each channel is to signals: Channel B observes more than Channel A does. This is exactly the conclusion we reached in Section 4.1.1 from the nature of the bad coincidences, information which should not be automatically correlated with the kpps rates. The fact that the high threshold ratios are very close to one does not necessarily discount this result. Remember that the high threshold rate counts any signals that surpass any of the three higher energy levels. While a signal of a given energy might reach to the third level on the less demanding Channel B, it would only need to pass the second level on Channel A to register as a high threshold hit on both channels. Thus we would expect the rates

[3] We comment that for observations 73 and 203, the low threshold (that is, the single photoelectron hit rate) data over $200\,ms$ contained highly irregular count rates in Channel B, which result in the abnormally large ratios that artificially raise the average ratio. We say artificially because the two points are clearly outliers compared to the rest of the data. Furthermore, the absolute rates for Channel A over $200\,ms$ (for Obs. 73 and 203) are almost identical to the rates of both A and B over $100\,ms$; something went temporarily wrong with B. If we exclude the ratios of 6.506 and 7.098 from the low threshold, $200\,ms$ average, we arrive at an average of 0.712, which is consistent with the low threshold $100\,ms$ rate average and with the rest of the low threshold ratios in the table.

to be more equal, and indeed they seem to be. In the low threshold case, a signal that barely passed the lowest level on Channel B would not reach the lowest on Channel A, leading to the disparity that we see.

4.2.1 Disparity Between Expected, Measured, and Recorded Rates

Though the kpps numbers are helpful in that they confirm our previous conclusions, in general the kpps rates present more problems than they solve. As Table 4.4 shows, there is no obvious relationship between the low threshold kpps rates and the single photoelectron rate as observed with an oscilloscope and pulse counter attached to Channel A of the OSETI box. Also given in Table 4.4 are the expected rates for the arrival of single photons, as derived from Equation 2.9; the rate of single photoelectrons as observed by the counter; and the low threshold kpps rate for Channel A over the $100\,ms$ interval for selected stars over three nights of observation in December of 2001.[4] A few minutes with a calculator reveal that there is certainly no easy proportionality factor linking the measured rates and the kpps rates, as one would expect. Nor is it certain that there is a linear relationship between the two at all, though rough scatter plots don't rule out the possibility. Even if there were a linear relationship, the question remains: where are the photons going? Both between the calculated and measured singles rates and between the measured and kpps rates, there is an attenuation of roughly two orders of magnitude, far more extinction than can be explained by the 10-15% efficiency of the photodetectors alone.[5]

Figure 4.1 gives the kpps singles rate versus visual magnitude for all stars with $m_V \geq 2$. We note immediately that there is a strong correlation between kpps rate and visual magnitude, despite the rather noisy lower portion of the plot. Before we discuss the line that quantifies this correlation, we note two interesting features of the plot: the row of data points at the top of the plot and the apparent upward curve away from the best fit line at low magnitudes. The former is most likely an effect of the electronics

[4] Recall that the low threshold kpps rate is purportedly the rate of single photoelectron arrivals, and so, theoretically, should correspond with the rate measured by the pulse counter.

[5] We must remember that the kpps and measured rates should be at most half the expected rate, assuming the beamsplitter is splitting evenly. The attenuation here is certainly more than a simple 50%, however, so the beamsplitter is probably not the main problem.

Night of [Date]	Obs. No.	m_V	Calculated Rate, kilo-photons/s	Measured Rate, kilo-counts/s	Kpps rate, A, 100 ms	% Efficiency
07-12-01	286	5.3	1.4×10^5	$(1.0 \pm 0.1) \times 10^3$	11.7	1.4
	290	7.8	1.4×10^4	100 ± 10	0.69	1.4
	287	8.6	6.9×10^3	45 ± 5	0.33	1.3
	284	8.7	6.3×10^3	51 ± 3	0.28	1.6
	289	10.1	1.7×10^3	11 ± 1	0.06	1.3
09-12-01	315	5.7	9.9×10^4	850 ± 20	12.28	1.7
	312	6.0	7.5×10^4	690 ± 30	8.44	1.8
	318	6.6	4.3×10^4	380 ± 20	3.62	1.8
	316	8.5	7.5×10^3	81 ± 3	0.51	2.2
	317	11.1	6.9×10^2	7.0 ± 0.4	0.07	2.0
11-12-01	329	4.4	3.3×10^5	$(2.3 \pm 0.04) \times 10^3$	197.20	1.4
	334	7.1	2.7×10^4	220 ± 10	2.89	1.6
	330	8.3	9.5×10^3	75 ± 3	1.11	1.6
	332	11.2	6.3×10^2	7.3 ± 0.3	0.05	2.3
	335	11.4	5.2×10^2	5.6 ± 0.4	0.06	2.2
22-12-01	439	9.0	4.8×10^3	46	0.31	1.9
	441	9.6	2.7×10^3	30 ± 1	0.23	2.2
	444	10.0	1.9×10^3	17 ± 1	0.13	1.8
	442	10.5	1.2×10^3	11 ± 1	0.13	2.2
	437	10.6	1.1×10^3	13 ± 2	0.06	2.4

Table 4.4: The calculated arrival rate of single photons, single photoelectron event rate ("Measured Rate"), kpps rates, and telescope efficiency as recorded by D.T. Wilkinson (ordered by date and visual magnitude). The calculated rates were obtained via Equation 2.9, with the numerical factor in the exponent taken to be 2.5 rather than 2.512 and $I_\circ = 3.5 \times 10^5$ photons/s for a 1 m telescope—a good approximation to our 36 in mirror; as before, m_V is the visual magnitude of the star. The efficiency is the ratio of measured to calculated rates, times two to account for the split beam; see Figure 4.2 for a plot of the measured rate versus visual magnitude that gives the best-fit efficiency. Observe the overall decline in measured hit rates and in kpps rates with increasing m_V. (The anomaly in the measured rates between observations 287 and 284 on 07-12-01 and the lower-than-average efficiency are most likely a function of the hazy sky that night.)

(see Figure 4.6), while for the latter we have no explanation (it appears also in the plot of hit rate versus magnitude, Figure 4.4). The predominance of noise below the line, however, is probably due to bad weather. Haze and clouds will always conspire to block photons from our telescope, while there are very few, if any, sources that could artificially enhance the signals.

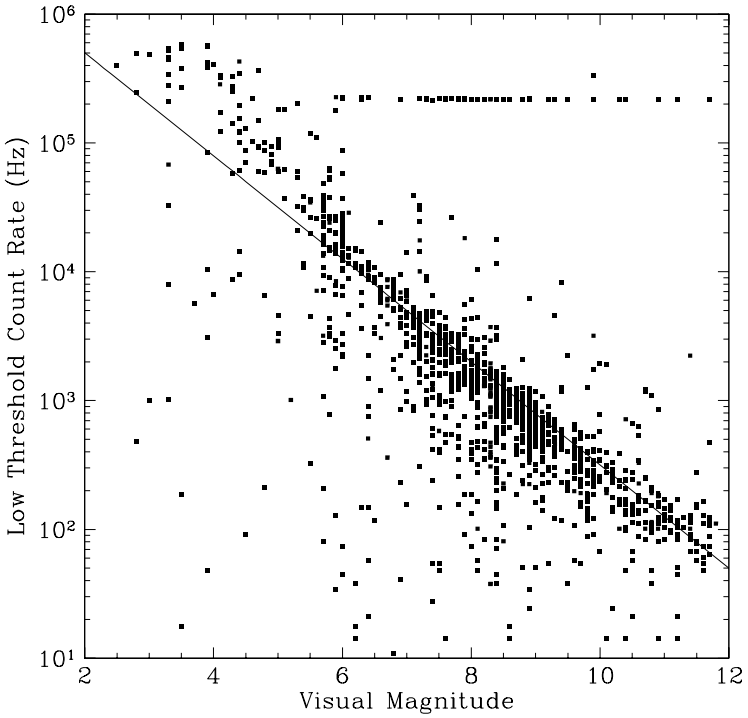

Figure 4.1: The low threshold kpps rates, in counts per second, versus apparent star magnitude for data taken at Princeton between November 2001 and early April 2002. Total kpps counts were obtained by adding the low threshold counts of each time interval in both detectors and dividing by $300\,ms$ to obtain the rate in Hz [15]. The best fit line of the data is $\log R_\gamma = -2/5 m_V + 6.5$, where R_γ is the singles count rate. Plot generated by C. Coldwell.

We turn to the best fit line, whose equation is

$$\log R_\gamma = -2/5 m_V + 6.5, \tag{4.1}$$

where R_γ is the observed arrival rate of single photoelectrons. To see how this compares to expectations, we derive the theoretical form of the equation below. The general equation is a variant of Equation 2.9, with the reference m_V taken at zero, not twelve [18]:

$$\log(F_T/F_\circ) = -2/5\, m_V, \tag{4.2}$$

where $F_\circ$ is the number of visual bandwidth photons per second through one square

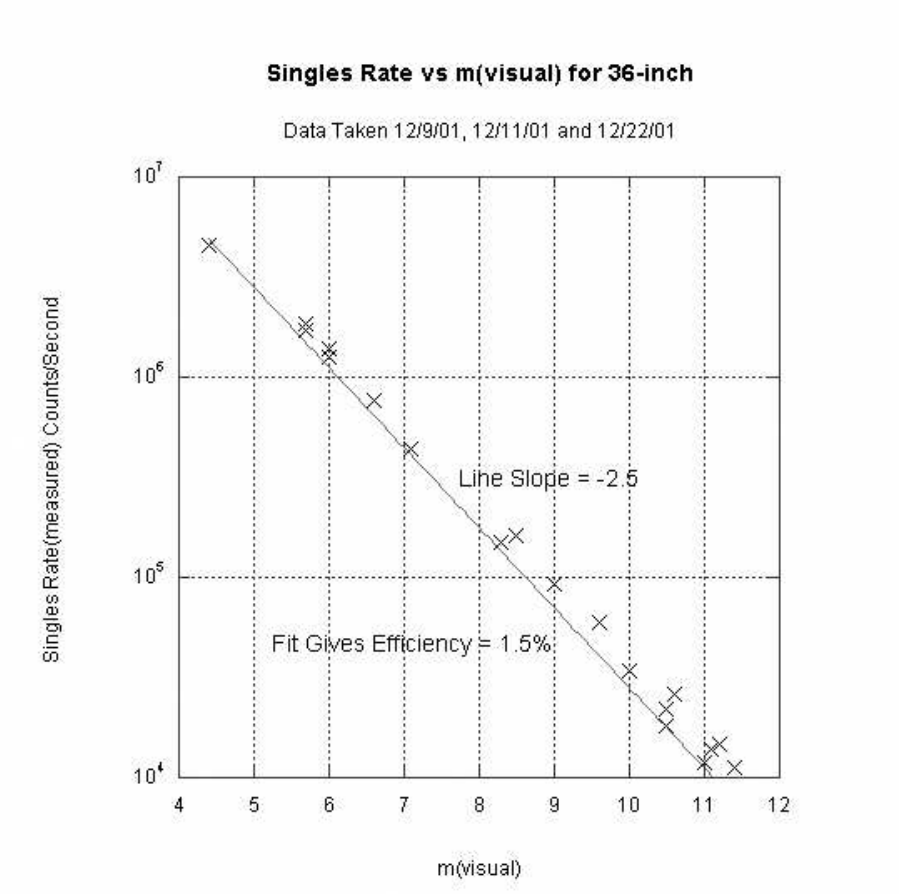

Figure 4.2: A plot of singles rates, as measured by an oscilloscope and counter attached to Channel A of the OSETI box, versus visual magnitude, for observations made the nights of 09, 11, and 22 Dec 01. Defining the slope to be -2/5, the best fit line indicates a telescope plus photodetector efficiency of 1.5%, on par with the individual efficiencies as calculated in Table 4.4. That the efficiency of the best fit line is lower than many of the calculated efficiencies is probably due to the high weight given to observation 329 ($m_V = 4.4$), whose efficiency was lower than the other points. Plot generated by D.T. Wilkinson.

meter from a star of magnitude zero. $F_T = F_m A$ is the flux of visual bandwidth photons through the Fitz-Randolph telescope, the product of our telescope area A and the flux F_m per second per square meter for a star of visual magnitude m. We can expand the

logarithm and rearrange to get

$$\log F_m = -2/5\, m_V + \log F_\circ - \log A. \tag{4.3}$$

$F_\circ$ is a constant: $F_\circ = 1.87 \times 10^{10}\, m^{-2}\, s^{-1}$, with $\log F_\circ \approx 10.3$.[6] For our telescope, we take the radius of the primary mirror to be $R = 35/2\, in = 0.45\, m$, so $A = 0.63 m^2$ and $\log A \approx -0.2$.[7] Therefore our theoretical best fit line is

$$\log F = -2/5 m_V + 10.5, \tag{4.4}$$

which is obviously not identical to Equation 4.1. The difference of four between the calculated constant in Equation 4.4 and the constant of the best fit line indicates that our kpps numbers are four orders of magnitude lower than the calculated flux rates, which is consistent with our observations regarding Table 4.4. The low efficiency of our telescope accounts for about two orders of magnitude (see Table 4.4 and Figure 4.2), but again we cannot immediately explain the further attenuation.

4.2.2 Possible Attenuation From the Telescope

With respect to the measured versus kpps rate discrepancy, we have no explanation at this time, but with respect to the difference between expected and measured rates, we can posit a solution. It is possible that some of the light is being blocked by the OSETI aperture itself, though this would not solve the problem entirely.[8]

Figure 4.3, Part B, shows the path that light takes once it has been directed through the hole in the primary mirror and is focused in front of the beam splitter. So that the

[6] $F_\circ$ is derived as follows from data in [18] (remember that $A = 1$ for an aperture of one square meter, and therefore $\log A = 0$). A zero magnitude star has an energy flux $3.75 \times 10^{-9} erg/(cm^2\, s\, \text{Å})$, and the visible spectrum has a width of $1,800$ Å. Thus the flux across the visible spectrum is 6.65×10^{-6}. Energy per photon is $h\nu = hc/\lambda$, and we use $\lambda = 5,500$ Å(the center of the visible band) to give us an average energy per photon of $3.62 \times 10^{-12} erg$. Combining everything, we have a flux of photons per second per square meter from a zero magnitude star. Taking the implicit area to be one square meter, the flux in photons per second defined as $F_\circ$ is $1.87 \times 10^{10}\, m^{-2}\, s{-}1$. This $F_\circ$ is the particular version ($m_V = 0$) of the F_T in Equation 4.2.

[7] We will see in Section 4.2.2 why we treat the diameter of the main mirror as 35 rather than $36\, in$.

[8] Of course, light will always be lost along the way, so we expect an efficiency much less than 100%. However, we do expect the telescope plus photodiode efficiency to be at least twice as high as it is; hence the "problem."

edges of the light cone are not shaved off, the beam focuses very close to the aperture, with the ideal focus virtually in the aperture itself at the telescope's focal distance of $F = 12.4\,m$. For a $36\,in$ diameter telescope ($M_D = 36\,in \approx 914\,mm$) with this focal length, a focused beam subtends a half angle of $\arctan(M_D/2F) = 0.037\,rad$. The primary baffle (cf. Figure 4.3, part A) has a diameter of $B_D = 5\,in = 127\,mm$ and is located only $L = 69\,in \approx 1752\,mm$ from the ideal focal point. The half angle of the widest beam that the baffle will allow through is only $\arctan(B_D/2L) = 0.036\,m\,rad$. Working backwards, this reduces the effective diameter of the primary mirror to about $35\,in$.

If everything is properly aligned along the horizontal and vertical axes of symmetry of the beam splitter, we can conclude from this maximum beam width that all the light that passes through the aperture should reach one or the other of the photodetectors in the OSETI box . Still assuming that the focal point is virtually in the aperture, we see from Figure 4.3, part B, that the photodetector is $4\,in \approx 101\,mm$ from the opening. Taking $\phi_{max} = 0.036\,rad$ to be the maximum half angle of the beam, we find that over a distance of $101\,mm$ the beam reaches a half-width of just under $3.7\,mm$, which is comfortably within the $4\,mm$ radius of the photodetector.

For the levels of inefficiency we see to be the result of misaligned equipment, the photodetectors would have to be very seriously misaligned. If they are off axis by their entire radius, less than half of the beam hits the photodiode. To this efficiency of $\approx 50\%$ we add the known efficiency of the photodetector, which reduces the overall yield to 5% or so. Since we have been dealing with fractions and not numbers, this 5% efficiency takes both detectors into account, and it is still more than twice the 1.4–2% efficiency we see in Table 4.4 and Figure 4.2.

There is one more possible source of attenuation from the telescope, and that is that the beam is shaved off by the final aperture, the opening into the OSETI box (see Figure 4.3). At a distance ε in front or behind the focal point in the aperture, what will the beam width be? In particular, how far in front or behind the aperture can the focal point be so as not to open wider than the diameter $a \approx 0.2\,mm$ of the aperture: $\varepsilon \tan 2\phi \leq a$? Here ϕ is the opening angle of the beam of light entering the telescope,

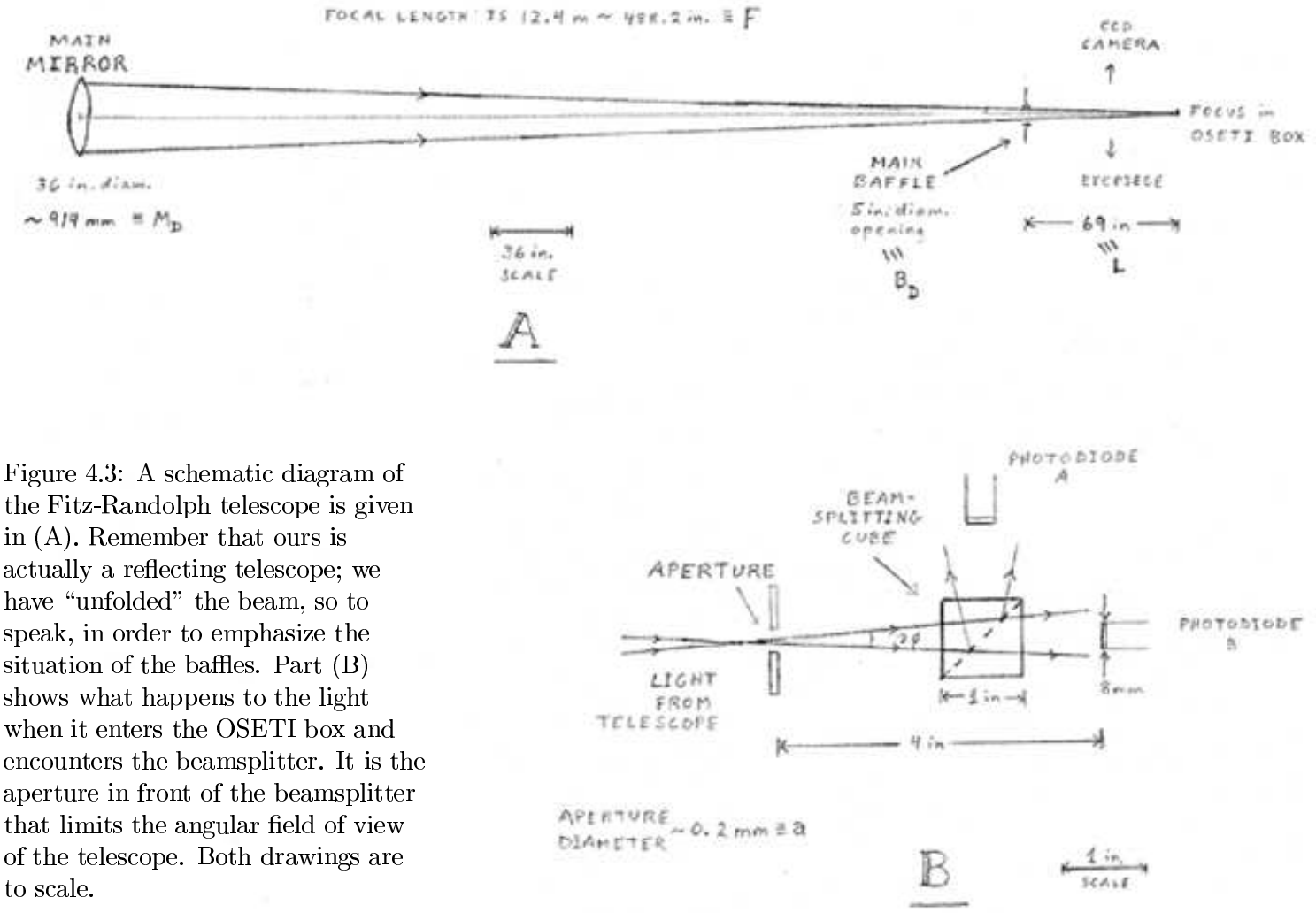

Figure 4.3: A schematic diagram of the Fitz-Randolph telescope is given in (A). Remember that ours is actually a reflecting telescope; we have "unfolded" the beam, so to speak, in order to emphasize the situation of the baffles. Part (B) shows what happens to the light when it enters the OSETI box and encounters the beamsplitter. It is the aperture in front of the beamsplitter that limits the angular field of view of the telescope. Both drawings are to scale.

and we have made the small angle approximation $2\tan\phi \approx \tan 2\phi$, which is valid for all the angles concerned here. The opening angle of the beam is given in terms of the telescope main mirror diameter and focal length,

$$\tan 2\phi \approx \frac{M_D}{F \mp \varepsilon_\pm}, \tag{4.5}$$

where ϕ was previously estimated to be $\phi_{max} = 0.036\,rad$ and ε_+ and ε_- are the allowed distances in front and behind the aperture, respectively ("in front" indicating closer to the main mirror). Thus

$$\varepsilon_\pm \frac{M_D}{F \mp \varepsilon_\pm} = a \tag{4.6}$$

provides the limiting conditions, and

$$\varepsilon_\pm \leq \frac{aF}{M_D \pm a} \tag{4.7}$$

gives us our maximum variations in focal length in either direction. Using a $35\,in$ diameter lens, we find that $\varepsilon_+ \leq 2.789\,mm \simeq \varepsilon_- \leq 2.790\,mm$. D.T. Wilkinson estimates that the focal point of the beam is within $2\,mm$ of the aperture, comfortably within the allowed variation of $\pm 2.7\,mm$ [36]. Thus if our telescope is focusing properly (which it is) we do not have to worry about the beam being attenuated by the aperture.

Based on the above calculations, it is highly unlikely that the unexpectedly low telescope efficiency is due entirely to mechanical misalignment of the telescope, though it is probably a contributing factor. Beyond that possibility, we have nothing further to posit at this time to explain why the OSETI circuitry is not receiving more photons.

4.3 Hit Rates: Expected and Actual

With the hit rates themselves, on the other hand, we have somewhat the opposite effect: far more coincidences than we would predict. But before we can compare our results to what we expect to see, we must define the latter. Note that henceforth in any numerical calculations we will take the photodetector efficiency to be 10%.

4.3.1 Photoelectron Pileup Rate to First Order

To that end we present a derivation of the Poisson distribution law, which governs the occurrence of rare events in a system that is randomly sampled, and use that formula to derive a probable limit on the frequency of coincidences we expect to see. First, recall that the energy thresholds in the Princeton OSETI box are set to correspond to the arrival of 2, 4, 8, and 16 photoelectrons for each channel. Since a coincidence theoretically requires that at least the lowest threshold of each channel be surpassed simultaneously, this translates to the arrival of four photoelectrons, two in each detector, within a few nanoseconds of each other. What we would like to know is the likelihood that such a four photoelectron "pileup" will occur, given the sampling time and the expected rate of photon arrival from a star.

Before reproducing a more rigorous proof, we can get a feel for the general form of the answer via the probability arguments touched upon earlier in Section 3.1.2. Consider a star whose photon flux translates to an average rate of r photoelectrons/s into our telescope (that is, the photon arrival rate is $10r$), and assume that we can "sample" the channels, using the MTD, at a rate of $1/\tau$, where τ is the time resolution allowed by the approximate length of one pulse, which itself is determined by the photodetector and the amplifiers. We take the pulse length to be about $10\,ns$; the circuit amplifiers limit the pulse rise time to a few nanoseconds. The probability of a photoelectron to arrive within a given interval τ is $r\tau$, while the probability of two photoelectrons arriving within the same interval is $(r\tau)^2$, since we are considering the probability of two ideally independent events. For two photoelectrons in each of the two detectors within the same time the probability is again squared, and we have a four photoelectron pileup probability of about $(r\tau)^4$. We assume here that both detectors are on equal footing, observing the same rates $r_1 = r_2 = r$ and sampling with the same interval; as we know, this may not be exactly the case. To find an expected event rate for the pileups, we multiply by the rate of sampling in the circuit, and thus obtain a four photoelectron event rate of

$$r_P \propto r^4\tau^3. \tag{4.8}$$

4.3.2 Photoelectron Pileup Rate and the Poisson Distribution

In the calculations that follow, we will obtain a more general result that will tell us the expected rate not only of four-photoelectron events, but also the rate of observing any events involving higher numbers of photoelectrons coincidences.[9] We begin with a derivation of the Poisson distribution, well known in statistics to find the probability of a small number of events in a process of repeated, random sampling [26].

We begin with a time interval t, which will eventually become our sampling time τ, and divide it into N segments, each lasting t/N. Justified by the knowledge that we will eventually take the limit as $N \to \infty$, we presume that t/N is small enough that only one photoelectron will arrive in that time. As above, the probability of a given event occurring in some time T is rT, where r is the rate. Our T is the t/N we just found, and therefore the probability of arrival of $n < N$ photoelectrons in time t (assuming no correlation between events) is

$$p_n = \left(\frac{rt}{N}\right)^n \left(1 - \frac{rt}{N}\right)^{N-n} \tag{4.9}$$

where we have multiplied the probabilities of either photoelectron arrival or non-arrival for each of N intervals. From the binomial expansion, we have the multiplicity function giving us the number of ways that n photoelectrons could distribute themselves in the N intervals:

$$\left(\begin{array}{c} N \\ n \end{array} \right) = \frac{N!}{n!(N-n)!}. \tag{4.10}$$

Thus the probability of any n photoelectrons in any distribution during the given interval is the product of the two equations above, or

$$P_n(t) = \frac{N!}{n!(N-n)!}\left(\frac{rt}{N}\right)^n \left(1 - \frac{rt}{N}\right)^{N-n} = \left(1 - \frac{rt}{N}\right)^{N-n} \frac{N!}{N^n(N-n)!}\frac{(rt)^n}{n!}. \tag{4.11}$$

We now validate our assumption that only one photoelectron will arrive in t/N by taking N alone to infinity. From the formula for the exponential, $e^{-s/N} = \sum_{m=0}^{\infty} \frac{(-s/N)^m}{m!}$, we

[9] This derivation follows that presented in [30] and [9].

approximate the expansion by the first two terms,

$$e^{-s/N} \approx 1 - \frac{s}{N} \quad \Longrightarrow \quad e^{-s} = \lim_{N\to\infty} \left(1 - \frac{s}{N}\right)^N. \tag{4.12}$$

We can substitute the exponential as we take the limit of Equation 4.11 since n is fixed while N grows without limit: $\lim_{N\to\infty}(N-n) = N$. In the limit of large N, the fraction $N!/(N-n)! \approx N^n$, so the fraction with the factorials reduces to one and we obtain

$$P_n(t) = \frac{(rt)^n e^{-rt}}{n!} \tag{4.13}$$

as the probability of n photons arriving in an interval t. Note that the factor of rt is in some sense a probability, but it is also equivalent to the average number of photons that we would expect to see in t—not necessarily the particular number n.

With the factor of $(rt)^n$ we can already see the first similarities between this expression and the qualitative function derived in Section 4.3.1: divide the $P_n(t)$ by the interval time t and substitute 4 for n, and we have reproduced Equation 4.8 except for some numerical constants. (In our case, $rt \ll 1$ in general, so $e^{-rt} \approx 1$.) We said we would like to be more exact, however, and find the combined probability of events involving four or more photoelectrons, so we shall.

Since we took the multiplicity of photoelectron configurations into account, we have counted every possible state of the system, and Equation 4.13 is properly normalized. To find the combined probability of m or more photoelectrons, we simply add the P_n:

$$Q_m(rt) = \sum_{n=m}^{\infty} P_n(rt), \tag{4.14}$$

where we have made P a function of rt rather than of t alone. Now, since the total probability is one, we can write

$$1 = \sum_{n=0}^{m-1} P_n(rt) + \sum_{n=m}^{\infty} P_n(rt), \tag{4.15}$$

or

$$Q_m(rt) = 1 - \sum_{n=0}^{m-1} P_n(rt) = 1 - e^{-rt} \sum_{n=0}^{m-1} \frac{(rt)^n}{n!}. \tag{4.16}$$

Using the same power series approximation for the exponential, we can eliminate the summation altogether, since $\sum_{n=0}^{m-1} \frac{(rt)^n}{n!} \approx e^{rt} - \frac{(rt)^m}{m!}$. Therefore, to leading order in m and in rt,

$$Q_m(rt) \approx 1 - e^{-rt} \left(e^{rt} - \frac{(rt)^m}{m!} \right) = P_m(rt) = \frac{(rt)^m e^{-rt}}{m!} \approx \frac{rt^m}{m!}. \tag{4.17}$$

We are right back where we started, with the probability of n *or more* events given almost exactly by the simple probability of n events. We have managed to wave away one of the numerical constants, at least for the time being, but since rt is always positive, a quick look reveals that the exponent will only decrease the probability: Equation 4.17 is an absolute upper bound. From this probability we easily obtain the expected rate of an m–photoelectron pileup by multiplying by the sampling time $1/\tau$ to get

$$R_m(r, \tau) = \frac{r^m \tau^{m-1}}{m!}, \tag{4.18}$$

where we have moved back to our original τ notation.

We are not quite finished, however, because this equation makes no distinction between the rate of two photoelectrons arriving in each detector, which would give us a coincidence, and four photoelectrons arriving simultaneously in one detector, which would not. The beamsplitter provides one further constraint on the system that reduces the rate in Equation 4.18 by a factor that is essentially another Poisson distribution. It is now helpful to think of the circumstances of an m–photoelectron event in a slightly different way: It is the rate of a single event times the probability that an $(m-1)$–photoelectron event ($P_{m-1} \propto (rt)^{m-1}$) will also occur during the given sampling time (which we recall is the length of the original pulse). In both our detector and in Harvard's a minimum number of photoelectrons must enter each of two detectors simultaneously to achieve a hit. For any m photoelectrons arriving almost instantaneously, the probability of $m/2$ photoelectrons in Channel A and $m/2$ photoelectrons in Channel B (or, "not

in Channel A") is $(1/2)^{m/2} \times (1/2)^{m/2} = (1/2)^m$. The number of ways they could distribute themselves evenly between the two channels is given by Equation 4.10 with m and $m/2$. Thus Equation 4.18 in its final form becomes

$$R_m(r,\tau) = \frac{m!}{(m/2)!(m-m/2)!}\left(\frac{1}{2}\right)^m \frac{r\, r^{m-1}\tau^{m-1}}{(m-1)!} = \left(\frac{1}{2}\right)^m \frac{m\, r^m \tau^{m-1}}{[(m/2)!]^2}. \quad (4.19)$$

4.3.3 Good and Bad Hit Rates at Princeton

We can now with impunity predict the expected rate of a random four photoelectron pileup, though we immediately run into results that do not match our nightly observations. Our standard example star ($m_V = 12$) has a photon arrival rate in our telescope of 3×10^5 per second, which translates to 3×10^4 photoelectrons per second, assuming 10% photodiode efficiency. With the time $\tau \approx 10^{-8}\ s = 10\, ns$, we get a "natural" four photoelectron event rate of about $(80 \times 10^{16} \times 10^{-24})/16\, s^{-1}$. This translates to one pileup every $2 \times 10^7\ s$, or once in 228 days. This seems fairly rare, but since the resolving time is fixed, the pileup rate grows as the fourth power of expected photoelectron arrival rate. We need a photoelectron rate of only 2×10^6 to achieve an expected pileup once every second, a rate that corresponds ideally to a star with m_V of only 7.4 (from Equation 2.9). We have never observed rates this high (our highest is 2,700 hits per hour) though we observe stars of magnitude as high as 2. If we take into account the additional order of magnitude between our expected and observed singles count rates (having already accounted for the attenuation factor of 10 from the photodetector), we would need a star with a photon arrival rate of 2×10^8 to achieve a pileup every second. However, such a star has visual magnitude 2.4 and is therefore still within our observational scope. As we see in Figure 4.4, there does seem to be some exponential correlation between the visual magnitude of a star and its rate of hits, yet few of the stars even approach the one-per-second rate that would be predicted (rates are given per hour, so an event per second is more than 10^3 events per hour). In an ironic twist, it is possible that whatever is causing the great disparity we see between the expected and measured singles rates and the kpps rates, which so perplexed us in Section 4.2, is actually saving us from a deluge of data.

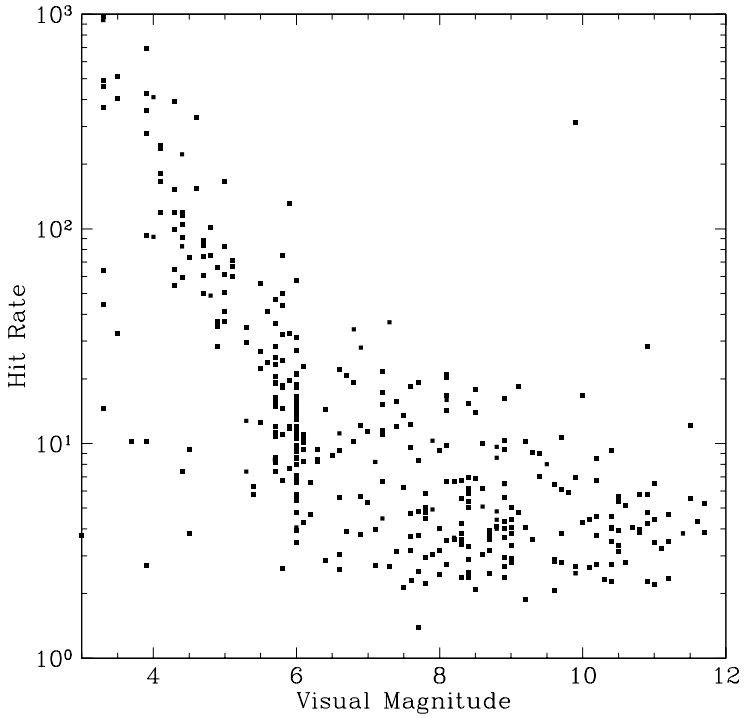

Figure 4.4: Total hit rate in counts per hour, versus apparent star magnitude for data taken at Princeton between November 2001 and early April 2002. Here, as in Figure 4.5, most of the stars were observed for less than one hour, meaning that there are large error bars on each point. The line plotted over the plot has a slope of -8/5, which is the expected slope of the best-fit line (see calculation at the end of Section 4.3.3). Plot generated by C. Coldwell.

With respect to Figures 4.4 and 4.5 themselves, we see first of all that the latter is extraordinarily noisy, to the point of being meaningless. Some explanation for that is given in the caption to Figure 4.5, and the variation in integration time probably explains much of the noise in Figure 4.4 as well. A saving point of Figure 4.5 is that the data points are not randomly distributed; if they were, the upper right and lower left corners of the plot would be as populated as the diagonal band separating the two corners. Noisy as it is, a curve fit to this plot would probably approximate the straight line expected from an exponential on a log plot. The plausibility of an exponential fit is greater when we look at Figure 4.4, which has more data points and is better distributed overall.

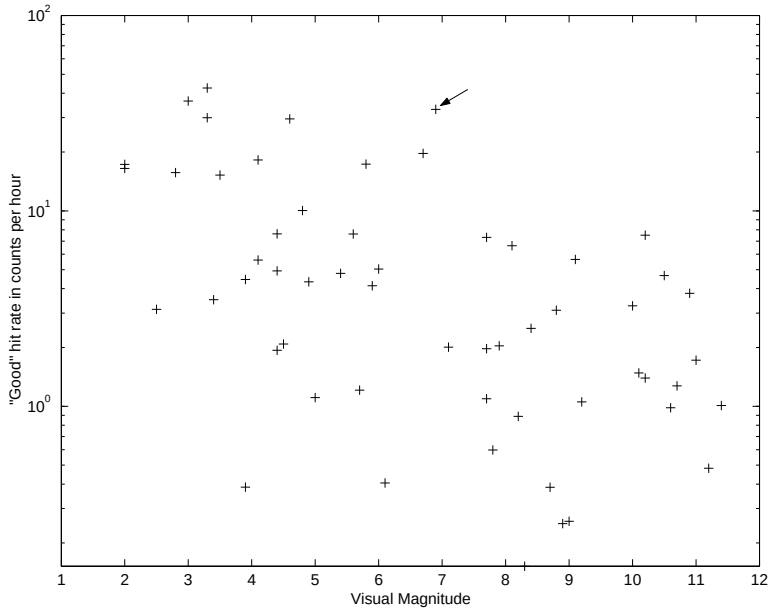

Figure 4.5: Good hit rate versus apparent star magnitude for data taken at Princeton between 1 Nov 01 and 28 Feb 02. The good hit rates are calculated over the total time a star is observed, possibly encompassing many observations over many nights. Though this has the effect of smoothing out anomalies in the long run, the rates by themselves obscure some of the details that help explain abnormally high rates. For example, the hit rate of 33 for a 6.9 magnitude star, indicated by the arrow, was caused by only one good hit: we observed the star for less than two minutes. Since our initial observation on 3 Jan 02, we have observed that star again (4 Apr 02), and its good hit rate, as of 16 Apr 02, is only 7. The uncertainties are such as to render this plot unusable for curve fitting.

Where Figure 4.1 had a slope of $-2/5$, we would expect that graphs both of good hits and of total hits versus m_V to have a slope of four times that, or $-8/5$. This comes from the Poisson distribution, where the rate of a four photoelectron pileup is proportional to the rate of arrival of one photoelectron (the singles rate) to the fourth power:

$$R_4(r,\tau) \propto r^4. \tag{4.20}$$

Since the photoelectron singles rate can be given by Equation 2.9 (relating the photoelectron arrival rate r to $r_\circ$, rather than relating the photon arrival rates), we have the

relation between R_4 and m_V,

$$R_4(r,\tau) \propto {r_\circ}^4 10^{4(-2/5)(m_V - m_\circ)}, \tag{4.21}$$

and the slope in Figures 4.4 and 4.5 should be an even multiple of the slope of the exponential:

$$\log R_4 \simeq 4 \log r_\circ + -8/5(m_V - m_\circ) + C, \tag{4.22}$$

where the additional constant term accounts for the other constants in Equation 4.19. Unfortunately, a cursory comparison of this plot to Figure 4.1, which has a slope of $-2/5$, is not promising: the plots of hit rate seem to have slopes that are shallower, not steeper than the kpps rate. A line of slope $-8/5$ is drawn over Figure 4.4, and the lack of a good fit is clear, at least for the portions of the plot at higher m_V. This indicates again that there is a strong attenuation of the signals between the photons entering our telescope and the entries into the data log. The only redeeming factor of these plots seems to be that the noise of both occurs primarily below the best fit curve (or where one would be, in Figure 4.4). This at least provides some link to the real world, as photons are more likely to be extinguished than multiplied (see Section 4.2.1).

4.3.4 Hit Rates at Harvard–Smithsonian

As we noted earlier when examining the causes of bad hits in the Harvard-Smithsonian data set, their hit rates are much smaller than ours. This is most likely because their lowest energy threshold is set at a three photoelectron level, rather than the two photoelectron level at Princeton. When Harvard sees a coincidence, they should be seeing a six photoelectron pileup, with the expected rate as calculated in Equation 4.19: $R_6(r,\tau) = r^6\tau^5/384$. Ironically, low as they are, Harvard's hit rates are much higher than the maximum predicted rate. For the same photoelectron arrival rate of 3×10^4 per second and a $10\,ns$ sampling time, Harvard should be seeing a pileup once every 167 million years or so. Obviously, this is not the case, and even for a twelfth magnitude star good hits are observed far more often. We do not have any data for the singles rates at Harvard–Smithsonian, but their low threshold kpps numbers, which supposedly

represent the singles rate, tend to be on the order of 10^3, further lowering the probability of a pileup. A plot for Harvard's low threshold kpps numbers is given in Figure 4.6. This plot, analogous to Figure 4.1 for the Princeton data, is striking in its dissimilarity: there is apparently no correlation whatsoever of kpps rate with star magnitude. Obviously this is an odd situation. The one similarity between the two plots is interesting, though: that the same horizontal line of data points at a high kpps rate appears in both indicates an origin in the electronics, perhaps some type of system saturation.

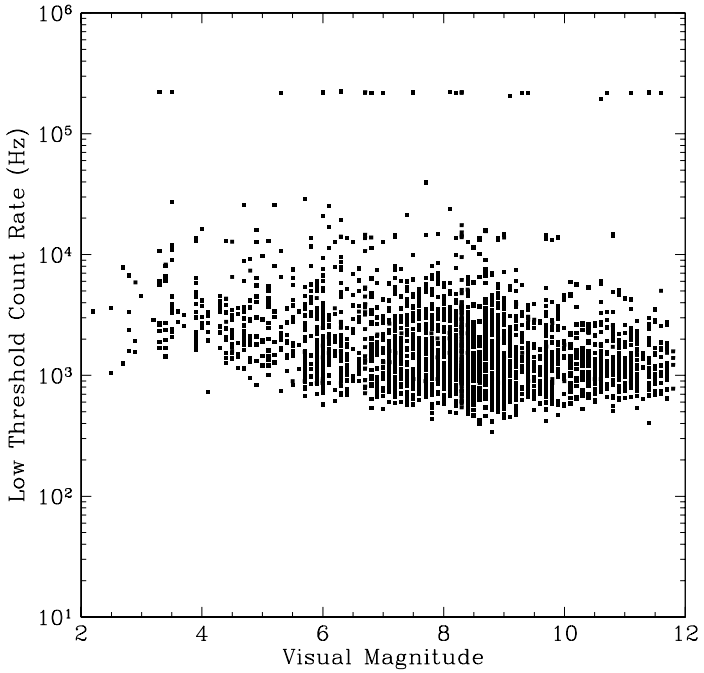

Figure 4.6: Low threshold (single photoelectron) count rate, in counts per second, versus apparent star magnitude for data taken at Harvard between November 2001 and early April 2002. Plot generated by C. Coldwell.

For these and other reasons, such as the lack of apparent correlation between the low and high threshold kpps numbers at Harvard, we are led to believe that their kpps numbers are more or less worthless. It is probable that most of Harvard's hits are due to instrument noise, primarily high voltage arcing in the the detector, for in addition to the lack of correlation of kpps to star magnitude, their hit rate increases in humid weather.

Chapter 5

Future Projects for OSETI

Before closing, we turn briefly to the future of optical SETI at Princeton and explore one way in which the experiment could be made more efficient. We can, of course, increase our efficiency by tracking down the bugs that are causing our unexpectedly high telescope attenuation and the additional mysterious disappearance of photoelectrons between the signal amplifier and the test circuit that gives the kpps numbers. However, we might also wish to move beyond the scope of the current experiment, as the Harvard–Smithsonian group is already doing.[1] To that end, we here provide a cursory exploration of the viability of observing star clusters in our galaxy, a method in use by the University of California, Berkeley, OSETI group [31].

5.1 Stellar Clusters versus Associations

The motivation for observing star clusters follows naturally from the experimental procedure currently employed at Harvard–Smithsonian–Princeton: the deliberate observation of individual stars as a means both of decreasing the percent of the sky we have to observe and as a way of immediately locating the direction of any detected signal. By observing stellar clusters, which might allow us to fit two or more stars in our OSETI aperture at any one time, we would obviously increase our rate of stellar observations. Though this is without doubt an advantage, stellar clusters present some challenges that

[1] They are currently building a "light bucket" telescope that will sweep the entire sky visible from Oak Ridge, rather than focusing on certain stars [23].

might not make them as attractive after all.

The prime candidate to spoil the scenario is the cluster density. A higher density would of course give us more stars, but it could also lead to a cumulative background luminosity that might be hard to overcome with the signals we anticipate. Further, a high cluster density implies a higher rate of close stellar encounters that adversely affect planet formation and could disrupt the stability of extant planet, neither of which is of course conducive to the long-term evolution of intelligent life.

Stellar clusters are not necessarily gravitationally stable. Clusters are often the result of one type of star formation, and many clusters drift apart by the time the stars would be old enough to have formed planets that could then host the evolution of intelligent life. Finally, we can apply these considerations only after picking out a subset of all clusters: those that are exposed, rather than being embedded in clouds of dust and gas, and those that lie within a reasonable distance of our sun (where we will show that "reasonable" corresponds to about $1.15\,kpc$). In the sections that follow, we will discuss whether clusters are known which would be good candidates for our observations.[2]

5.2 Stellar Clusters

The realm of stellar clusters (again considering only the subset of exposed clusters) is generally divided in two: open and globular clusters. The former contain Population I, or metal rich, stars, while the stars in the latter are classified as Population II, or metal poor [25].[3] Globular clusters, as indicated by their metal poor status, tend to be old (their stars formed while the universe largely lacked heavy elements) [4], giving them

[2]We restate that we would need to look at collections of stars that are gravitationally bound, to ensure groups that are concentrated enough to increase the yield in our field of view and to ensure that the same groups are old enough to have evolved advanced life. Stellar associations appear similar to clusters, but their members are moving away from each other too rapidly to remain a coherent unit for long. Our sun was probably once a member of an association [25], but now, five billion years and eight planets later, it is relatively isolated. Therefore, given that we would like to observe stars that have a reasonable chance of hosting planets, we reject observations of stellar associations: when the objects are of sufficient density to make them interesting, their members will be too young.

[3]The adjective "metal" refers to any of the elements heavier than hydrogen or helium.

plenty of time to have acquired planetary satellites.[4] On the other hand, the presence of heavy elements is necessary to form planets. Thus we are more likely to find planets around metal rich stars, which in turn tends to imply that we should look at stars in open clusters. There are exceptions to any generalization, though, so we will not on these grounds rule out either globular or open clusters.

5.2.1 Calculations of Stellar Density in Clusters

Before looking at long lists of the clusters themselves, we wish to satisfy ourselves that setting our sights on clusters is indeed a worthwhile pursuit that would increase our observational efficiency. To that end we will take as examples the globular cluster M13 and the open clusters Hyades, h Persei, and M11 and assess the density of stars that each would yield within the effective field of view of our telescope.

The largest potential difficulty with globular clusters is in fact their huge core densities, not their metal poor status. Globular clusters tend to have stellar populations between 10^4 and 10^7 in primary concentrations that are only $7.8\,pc$ ($28\,ly$) across, for a typical cluster like M13 [2]. For a spherical distribution, this translates to a plausible stellar density of $\approx \frac{10^5\ stars}{4\pi/3(3.9\,pc)^3} \approx 400\ stars/pc^3$. (Given in Table 5.1 are the distances, diameters, and number of stars of selected globular clusters.) The absolute density of the clusters is important when considering the viability of planet survival. Adams, in his discussion of the effect of open clusters on star formation, cites from [7] the probability P_D of encounters between stars that could seriously disrupt their solar systems as

$$P_D \approx \langle n \rangle \sigma v\,(\Delta t), \tag{5.1}$$

where σ is the scattering cross section, equal to $(200\,AU)^2 \approx 9.4 \times 10^{-7} pc^2$; v is related to the cluster radius R by $v^2 = GM/R$, where we have equated kinetic and potential energy; and Δt is the total lifetime of the cluster, with $\Delta t \propto (R/v)N/\ln N$. Thus

[4] Though [2] gives the specific ages in log years for certain globular clusters, the exponents vary only from 9.9 to 10.2, and general estimates of cluster ages set them all between 11 and 13 billion years old [25], while Binney and Merrifield note that they could be as old as 15 billion years [6].

GLOBULAR CLUSTERS

I

Cluster	NGC	Distance (kpc)	R_{HL} (arc min, $'$)	(pc)	Total m_V
M3	5272	13	1.2	4.6	6.4
M13	6205	7.7	1.7	3.9	5.9

II

Cluster	NGC	Distance (kpc)	R_{total} (arc min, $'$)	R_{HL} HL, (pc)	Total m_V
M4	6121	1.9	13.1	2.02	5.76
	6366	3.7	4.1	1.68	8.88
	6397	2.2	12.8		5.75
	6544	2.3	4.4	1.18	8.07
M22	6656	3.2	12		5.07

Table 5.1: A selected list of globular clusters in and around the Milky Way galaxy. Distances are measured with respect to the sun—essentially the distance from the earth. The length R_{HL} is the half light radius of the cluster, within which half of the total flux of the object emanates [3]. In II, angular radii refer to the entire cluster, not only the central concentrated regions. As stated, the number of stars in a globular cluster is usually between 10^4 and 10^7. Part I adapted from [2]; Part II from [27], with R_{HL} derived from [18].

Equation 5.1 reduces to

$$P_D \approx \frac{N^2 \sigma}{R^2 \ln N}. \tag{5.2}$$

For $N = 300$ and $N = 1000$ Adams quotes $P_D \approx 10^{-2}$ and 10^{-1}, or 1% and 10%, respectively. Thus the probability of "disruptive close encounters" [1] is not significant for $N = 300$, but it becomes so for $N = 1,000$. As Adams notes, $N = a\ few\ thousand$ will result in a significant probability for all the stars in the cluster to experience disruptive encounters, effectively eliminating the possibility of stable solar systems such as life requires. We emphasize that while the radii of globular clusters are usually of the same order of magnitude as the radii of open clusters, the populations of globular clusters are usually higher by two to three orders of magnitude, and the central members of globular clusters will not in general be conducive to planetary stability. For M13, for example, we have an estimate on its core population of $N \approx 10^5$ stars in a radius of $3.9\,pc$: there is certainly no possibility of undisturbed planets. These results do not necessarily hold for the less dense outer regions of globular clusters, for which we have no exact popula-

tion information. It is probable, however, that the outer regions of such clusters would have densities, and therefore interaction probabilities, low enough to allow stable solar systems. Thus, assuming that stars in globular clusters could form habitable planets, we would have to observe the edges of the clusters, beyond the half–light radius given in Table 5.1.

Density in the Periphery of Globular Cluster M13

To obtain an order of magnitude estimate for the stellar densities for an average cluster, we turn again to M13 which actually contains several factors of 10^5 stars in its total angular diameter $2R_f$ of about $16.6' \approx 37\,pc$ [27]. We will assume a total population of $N = 5 \times 10^5$, which is somewhere between "several 100,000 stars [and]...'more than a million'" [33]. We will further assume that all the stars have the same mass, with mass directly proportional to luminosity: therefore the half light radius refers also to the half mass radius and the half population radius (this is a common assumption, but Figure 5.1 shows that it is not, of course, entirely accurate[5]).

With the half–light radius given as $3.9\,pc$ by Table 5.1, we will make the further assumptions that the density within this radius is uniform, and that the density outside this radius is also uniform (remember, this is a rough calculation). Thus

$$\begin{cases} \rho_{HL} \approx \frac{N(3/4\pi)}{2{R_{HL}}^3}, & r < R_{HL}, \\ \rho_f \approx \frac{N(3/4\pi)}{2({R_f}^3 - {R_{HL}}^3)}, & r > R_{HL}. \end{cases} \tag{5.3}$$

For the numbers given above, the inner density $\rho_R \approx 10^3\,pc^{-3}$, which is too large for stable solar systems, while the outer density $\rho_f \approx 10\,pc^{-3}$. The outer density thus would yield a low disturbance probability (remember that we would also be using the larger of the two radii, R_f, in Equation 5.2). M13 is $7.7\,kpc$ away: in angular measures we have $R_{HL} = 1.7'$ and $R_f = 8.4'$, leaving, conservatively, an annulus of $6'$ within which we could conduct our observations. The diameter of the OSETI aperture in arc seconds is

[5]The same figure shows the shortcomings of many of the estimates we are about to make: the density can only really be considered uniform in the very center of the core region, outside of which it drops off sharply. By assuming a uniform density outside the core radius, we simplify the situation immensely, but our surface density behaves as a hyperbola, the rate of change in density increasing with radius. The actual surface density will fall off as $1/r^2$.

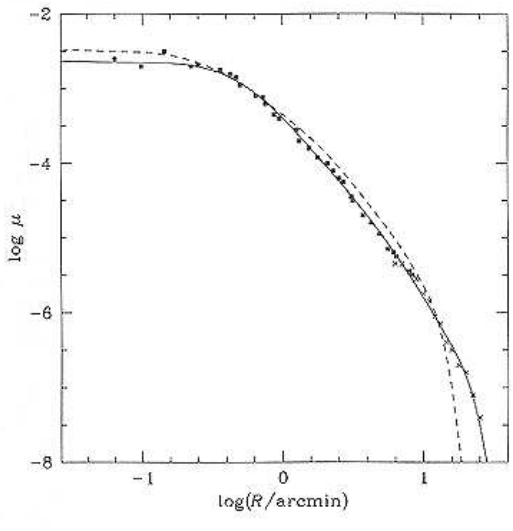

Figure 5.1: Surface brightness μ versus radius for the globular cluster M3, which is similar in size and luminosity to M13. Luminosity is a rough indication of stellar mass, and therefore we see the sharp decline in cluster population density as we move out from the core. The solid best-fit line assumes variation in stellar masses, while the dotted line is based on a model in which all masses are equal. The former is clearly a better fit. Figure taken from [6].

about $25''$, so we would have no difficulty concentrating on one small part of the cluster and avoiding the overly dense central core.

We next wish to know how many stars might appear in our field of view, were we to observe in the annular region (we retain the assumption of spherical symmetry and uniform density in the annular region). At a radius $R_{HL} < r < R_f$, the depth d of the cluster is

$$d(r) = 2\sqrt{{R_f}^2 - r^2}, \tag{5.4}$$

where distances are in pc. Thus at a radius r from the center of the cluster, we would have within our field of view N_g stars, where

$$N_g(r) = \rho_f d(r) \sigma_v, \tag{5.5}$$

and the subscript g indicates a globular cluster. At the distance of M13, our angular field of view means our telescope would observe a linear area of $\sigma_v \approx 0.7 pc^2$. For a

radius $r = 10\,pc$, or $4.5'$, from the center, we observe a cluster volume $d(r)\sigma_v$ of $20\,pc^3$, putting 200 stars in our effective field of view. The increase in observation efficiency is clear, even if we observed at a single radius around the cluster core.

Open Clusters

II

Cluster	NGC	Distance (kpc)	Radius R (arc min, $'$)	(pc)	Number of stars	Total m_V	log age (years)
Hyades		0.04	200	2.5	185	0.6	8.8
h Persei	869	2.2	12.5	8	29	4.1	7.0
M11	6705	1.7	6	3	300	6.3	7.9

II

Cluster	NGC	Distance (kpc)	Radius R (arc min, $'$)	(pc)	Number of stars	log age (years)
	2158	4.9	2.5	3.5	$400^{\dagger}$	9.04
Trumpler 5		2.4	3.5	2.8	$500^{\dagger}$	9.10
M67	2682	0.7	14.5	3.2	$356^{\dagger}$ *or* $200^{\ddagger}$	9.60
	6819	2.2	2.5	1.6	$487^{\dagger}$	9.54
	7789	1.9	7.5	4.4	$1362^{\dagger}$ *or* $400^{\dagger}$	9.20

Table 5.2: A selected list of open clusters in and around the Milky Way galaxy. Distances are measured from the sun to the cluster. Radii give, to the best estimate, the total cluster radius, all of which we may consider to be the core. The "log age" gives the power of ten of the star's age (a log age of 7 means an age in years of 10^7). In (II) we have included only clusters of ages greater than $10^9\,years$ within $5,000\,pc$ of the sun, whose richness classifications is 5 (meaning stellar populations greater than 250). We have further eliminated clusters in the southern hemisphere, as they would not be visible from our telescope. Total m_V was unavailable for the clusters in (II). Entries in (I) were compiled from [2] and [6], with the number of stars obtained from [24]. Entries in (II) were compiled from [27], [24], and [18]; sources of cluster populations are indicated by a † for [24] and a ‡ for [18].

Densities in the Open Clusters the Hyades, h Persei, and M11

By choosing to observe open clusters, we immediately avoid most of the problems posed by the high densities and low metallicities of globular clusters. Open clusters have populations in their more concentrated regions on the order of only 10^2. Indeed, a cluster that contains as few as 250 stars is defined as "rich," class 5 out of five where a 1 is poor [24]. Open clusters often have diameters of about $7\,pc$ [2], putting them on par with the core radii of globular clusters. Such dimensions give us a mean stellar density,

for a population of 185 stars in the Hyades (see Table 5.2, of $\frac{185\,stars}{4\pi/3(2.5\,pc)^3} \approx 3\,stars/pc^3$, or more than 300 times less dense than M13, the globular cluster just discussed. Immediately we see that the densities of open clusters are favorable to planetary formation even into the core of the cluster.

The lower densities of open clusters might be too low to help us, however. The 180 or so core stars of the Hyades[6] are scattered across an area whose diameter of $\approx 25,000''$ is 1,000 times larger than the $25''$ diameter aperture through which we make our observations. Thus it is highly unlikely that we would be able to observe more than one or two stars in the cluster at one time, giving us no increase in observation efficiency.

Clusters such as h Persei and M11 might be better candidates for our observations (even though h Persei has fewer stars, its angular radius is far less than that of Ursa Major, while M11 has an even smaller solid angle with a larger number of stars). Assuming uniform density throughout the cluster, we have stellar densities of $0.014\,stars/pc^3$ and $2.7\,stars/pc^3$ for those two clusters respectively. The observed area in pc^2 at a distance D is $\sigma_v = \pi(D\theta/2)^2$, where $\theta = 1.2 \times 10^{-4}\,rad$ is the angular diameter of the OSETI aperture. The number of stars in our field is still given by the general form

$$N_o(r) = \sigma_v \rho_R d(r). \tag{5.6}$$

However, ρ_R and $d(r)$ are simplified because of our assumption that for open clusters, the entire cluster is the "core:" we don't consider an intermediate half light radius between $r = 0$ and $r = R$. Thus $d(r)$ is found by Equation 5.4 with R in place of R_f and the cluster density is given simply by

$$\rho_R = \frac{N}{4\pi R^3/3}. \tag{5.7}$$

We have, then,

$$N_o(r) = 2\sigma_v N \frac{\sqrt{R^2 - r^2}}{4\pi R^3/3}. \tag{5.8}$$

[6]Binney and Merrifield [6] report that there are 200 stars in the cluster. There is often significant disagreement about the population of open clusters: tallies are complicated by the location of the clusters in the galactic plane, which obscures our view of the clusters.

The results of these calculations for the open clusters h Persei and M11 are summarized in Table 5.3. Though h Persei is not a good candidate, at $r = 0$ M11 yields an efficiency better than picking one particular star for observation.

	h Persei	M11
$\rho_R \; stars \; (pc^{-3})$	0.014	2.7
$\sigma_v \; (pc^2)$	0.6	0.3
$\mathbf{N_o(r)}$	**0.01**	**5.1**

Table 5.3: Estimates for the number of stars in our telescope's field of view at the center of two open clusters, h Persei and M11.

5.3 Evaluation of Stellar Cluster Observations

We are now equipped to evaluate globular and open clusters as candidates for observation. Beyond the density considerations, we require that the clusters be able to satisfy the limitations on power (calculated in Chapter 2) for transmitted and received signals. Here, that requirement manifests itself as a limit on the distance of the cluster from our sun. Equation 2.10 assumes, for our sample transmission wavelength, an extinction radius of $R_E = 1.15\,kpc$, at which even a directed signal will drop to half its original intensity. At that distance the beam would still subtend a radius of at least one AU. Our first requirement, then, is that any possible transmission source be within $1.15\,kpc$ of our sun. This distance requirement also limits the apparent magnitude of any object we might wish to observe. Assuming the broadcast power to be $10^{15}\,W$, as we did in Section 2.2.2, the number of photons per second received by our $1\,m$ telescope ($D_R = 1\,m$) from a source $1.15\,kpc$ away is 3.6×10^7 photons/s. This is still bright enough to overcome the background of a star or cluster with $m_V \approx 6.7$. For distant clusters, therefore, we place the extra constraint that they be fainter, with an apparent magnitude greater than 6.7.[7]

The relatively high peripheral densities of globular clusters, compared to open clusters, and the clusters' age make globular clusters attractive. However, the proximity

[7] *Revised 27 May 2002.*

requirement just derived from power considerations unfortunately eliminates any globular clusters from our list of targets for observation. Table 5.1 (II) gives five globular clusters that are close to our sun: the closest is still $1.9\,kpc$ away, more than 50% farther than our maximum allowed radius. Given the assumptions we have made about the technological capabilities of any transmitting civilization, it is not likely that globular clusters would be the source of signals of the type we seek. Until we are able to increase the definition of "reasonable" technology, we reject observations of globular clusters.

The prospects provided by open clusters are not much more optimistic. Given their low stellar populations, observing open clusters is often not better than observing single stars. However, some clusters do have high enough densities to make them worthwhile. There is a wide range in cluster densities: Binney and Merrifield [6] mention that the density in open clusters can vary from $\sim 0.1\,stars/pc^3$ (just slightly above the average density of the stellar field) to $\sim 10^3\,stars/pc^3$, which is on par with the globular clusters we looked at in Section 5.2.1.[8] Since the motivation for observing clusters rests almost entirely on a high stellar density in our field of view, a function that depends on cluster radius and distance from us as well as population, any open clusters we wanted to observe would have to be evaluated on a case by case basis.

We can limit the field of open clusters by imposing the requirements of distance and, additionally of age. Though the higher metallicities of open clusters are more conducive to the formation of planets (as mentioned above), it would be unreasonable to observe clusters with ages less than that of our solar system, that is, on the order of $10^9\,y$. The density in our solar neighborhood of open clusters (not their stellar constituents) falls off sharply with increasing cluster age [6], and Figure 5.2 shows that relatively few of the open clusters that have been catalogued reach even the age of our young sun.

A look back at Table 5.2 (II) virtually seals the demise of open clusters as targets of our telescope: only one cluster in the tables of [24] and [18] is rich enough, old enough, and close enough to satisfy us. Even this cluster is not particularly rich, and its very proximity drastically decreases the number of stars we would enclose in our field of view.

[8] Binney and Merrifield do not cite their source for this range in cluster densities. We quote it with the caveat that nowhere in the tables of [18] do we find a cluster with membership greater than 300. In the tables of [24] there are clusters listed with membership in the thousands, but such numbers are often much higher than would be implied by their richness classification, as assigned by Janes and Adler.

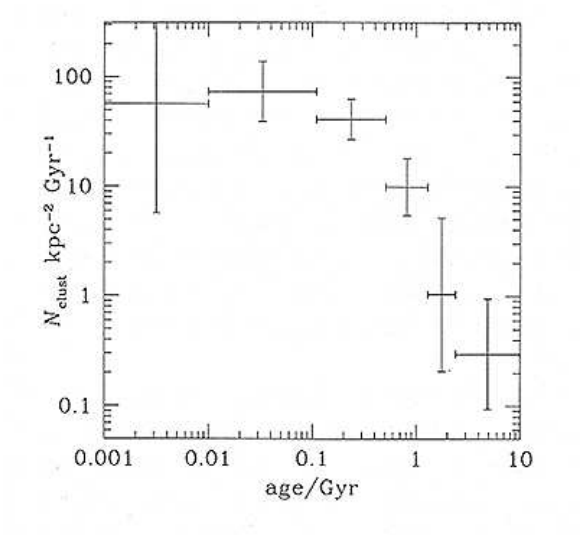

Figure 5.2: The correlation between the age of open clusters and their numerical density, for clusters relatively close to the sun. Figure taken from [6].

Based on the above analyses and calculations, we conclude that neither globular nor stellar clusters are particularly good candidates for observation at this time. The few clusters that might be feasible are open clusters at radii less than 1.15 kpc, but a further search through more versatile catalogues must be performed to find more appropriate candidates.

Chapter 6

Recommendations and Conclusion

Having concluded that stellar clusters are probably not the most promising avenue for future observations, we return to the current OSETI experiment and its difficulties. The analysis in Chapters 2–4 raises three primary questions about the current experiments at Princeton and Harvard:

1. Are the hits we are seeing being properly discriminated by the electronics, and are they being properly analyzed by the criteria in the software?
2. Where are the photons going? Can we come up with better explanations for the attenuation of four orders of magnitude by the time the kpps numbers are read out?
3. Are the experimental setups at Fitz-Randolph and at Oak Ridge compatible?

We cannot hope in this conclusion to answer all these questions. Instead, we will set forth the logical steps that might be taken to answer them, to the benefit of the experimental collaboration.

To the first question, though we do have an answer: The hits are neither properly discriminated nor analyzed. We recommend first that the criteria for good hits be expanded to exclude explicitly hits with an isolated rise or fall time of zero in any

threshold. However, we recommend also that we watch the hits for events whose fall times on both channels are all zero. Such a hit could indicate a very long, high intensity pulse, and we would not want in effect to miss the forest for the trees.

We should look into the occurrences of large numbered rise and fall intervals produced by the MTD, as well as its true ability to synchronize the intervals on multiple channels to the equivalent of $0.625\,ns$. If the MTD is found to be not quite as precise as we have been led to believe, perhaps we could relax the good hit criteria requiring the rise and fall numbers produced by the MTD to advance absolutely in time. Thus otherwise good hits would not be dismissed by jitters of only one or two nanoseconds in the MTD's fast timer.

To ensure that the coincidence and hot event discriminator circuits are working correctly, we should at the first opportunity test the reference voltage levels in all parts of the circuit, as well as the gain of the amplifiers and probably also the efficiency of the photodetectors. We need to ensure that our two channels are as closely matched as we can make them before discussing other possible explanations for the channel imbalances seen in Section 4.1.1.[1]

With respect to the second question, the drop by a factor of ≈ 100 between the singles rates measured by the external counter and the kpps numbers is particularly disturbing. The kpps numbers, aside from their appropriate log-linear relations to star magnitude, seem to bear little obvious relation to any other data that we gather. Our priority should be to determine what in the circuitry is bringing this about, an understanding that hopefully will come with a better comprehension of how the signals that get read as the kpps rates propagate through the electronics.

We have identified a signal attenuation of two orders of magnitude related to the telescope itself and to the photodetectors. Assuming that the latter do operate at 10% efficiency (a factor which should be confirmed, as mentioned above), that implies a telescope efficiency of only 10%. Such a low number is unexpected, as we have seen, and if it is accurate, it implies significant misalignments of the telescope mirrors and/or

[1] We ought also to make sure that the hot event discriminator will not eliminate high-voltage signals propagating through both channels simultaneously. That would involve the replacement of the OR gate currently in use with an XOR gate; we want the flexibility to observe any signals of unexpectedly high energy. *Recommendation added 27 May 2002.*

the beamsplitter and photodetectors in the OSETI box. Thus we recommend that the telescope and OSETI box be checked to ensure that they are all properly in line and well-focused. We might also want to do an analysis of atmospheric extinction of photons when observing at different zenith angles, but the telescope itself should be checked first.

Though any change in the good hit criteria in the software would necessarily affect both groups, the compatibility of the Princeton and Harvard experimental setups is obviously not a matter for Princeton alone to address. However, we can do our best to put the Fitz-Randolph telescope and observing equipment in the best shape possible, as described above. Perhaps when checking the reference voltage levels we might also adjust our thresholds to correspond to the 3, 6, 12, and 24 photon levels at which Harvard's thresholds are supposedly set; that would remove at least one potential explanation for hit rate and kpps rate differences and allow us to concentrate on other possibilities. In the spirit of experimental equality, and with reference to the horrendous kpps rates that Harvard records, we strongly encourage the team at Oak Ridge to perform similar checks on their system.

It is highly unlikely that all the discrepancies and abnormalities we see in the experimental data will be cleared up simply by following the recommendations above. However, given the analyses in the preceding chapters, it *is* likely that we will shed light on the primary problems by considering these suggestions. We look forward to further investigations and to the improved results we hope they will produce.

Appendix A

Physical Constants, Notation, and Conversions

CONSTANT	NOTATION	VALUE
Planck constant	h	$= 6.6 \times 10^{-27}\, erg \cdot s$
		$= 6.6 \times 10^{-34}\, J \cdot s$
speed of light	c	$= 3 \times 10^{8}\, m/s$

UNIT	NOTATION	CONVERSION
ANGULAR MEASURES		
one radian	$1\, rad$	$\approx 3438'$
one arc minute	$1'$	$\equiv 60''$
one arc second	$1''$	$\approx 4.85 \times 10^{-7}\, rad$
	2π radians	$\equiv 21,600'$
ENERGY, POWER, AND VOLTAGE		
one joule	$1\, J$	$= 10^{7}\, erg$
one erg	$1\, erg$	$= 10^{-7}\, J$
one watt	$1\, W$	$= 1\, J/s$
one volt	$1\, V$	$\equiv 1\, J/\text{coulomb}$

UNIT	NOTATION	CONVERSION
	TIME	
one year	$1\,y$	
one second	$1\,s$	
one millisecond	$1\,ms$	$= 10^{-3}\,s$
one microsecond	$1\,\mu s$	$= 10^{-6}\,s$
one nanosecond	$1\,ns$	$= 10^{-9}\,s$
one picosecond	$1\,ps$	$= 10^{-12}\,s$
one femptosecond	$1\,fs$	$= 10^{-15}\,s$
one megahertz	$1\,\mathrm{MHz}$	$= 10^{6}\,s^{-1}$
one gigahertz	$1\,\mathrm{GHz}$	$= 10^{9}\,s^{-1}$
	DISTANCE	
one angstrom	$1\,\mathrm{\AA}$	$= 10^{-10}\,m$
one millimeter	$1\,mm$	$= 10^{-3}\,m$
one centimeter	$1\,cm$	$= 10^{-2}\,m$
one inch	$1\,in$	$\equiv 2.54 \times 10^{-2} m$
one meter	$1\,m$	
one astronomical unit	$1\,AU$	$\approx 1.5 \times 10^{11}\,m$
one light year	$1\,ly$	$\approx 10^{16}\,m$
one parsec	$1\,pc$	$\approx 3.26\,ly$

Appendix B

Further Evaluation of the Kpps Data

In the weeks following the first publication of this paper on 29 Apr 02, we have received new information regarding the kpps data from Harvard–Smithsonian. These data, presented below, reveal that there are indeed serious abnormalities in Harvard's kpps numbers, though there are also periods when the detector produces numbers that correlate with star magnitude.

The persistently aberrant signals at Harvard seem to have been a result of misalignment of their OSETI aperture. An examination by P. Horowitz and C. Coldwell on 5 May 02 of the setup at Oak Ridge revealed that their box was seriously misaligned [10]. The alternations between periods of relatively good data and poor data seem to relate directly to work done on the telescope or on the OSETI box. In October of 2000, for example, the telescope's main mirror required maintenance, after which the OSETI box was re-attached and carefully aligned [16]; in November 2000 we see a significant improvement in the data (Figure B.5, as compared to Figure B.4). Likewise, in April 2001 the box was removed and replaced out of exact alignment. For the months shown in Figure B.6, which begins in April 2001, the data follow the best-fit line somewhat in May 2001, but there is significant deterioration in June 2001 and in the following months. It may be that the events surrounding the lightning strike in June 2001 worsened the situation, but there can be little doubt that misalignment has been the root problem. Since the box was checked on 5 May 02, Harvard's hit rates as seen daily by the author do seem to be much higher and closer to those at Princeton, though a detailed analysis

of the more recent kpps numbers has not yet been done.

The realization that the Harvard OSETI box was not properly aligned resolves the confusion surrounding Figure 4.6. Though it is very disappointing that Harvard has not been looking at stars since June of last year, the data are not entirely worthless since they give us insight into the detector itself. We can infer that the OSETI box itself produces background signals at the rate of about 10^4 Hz in summertime and 10^3 Hz in winter [16]. Since this background is entirely due to the OSETI circuit, Princeton can probably expect comparable backgrounds from its own circuit though we have not had occasion to observe the detector noise on its own.

If the Princeton box did produce a background comparable to that seen at Harvard, we would have a better explanation for the significant noise in Figure 4.1 and for the minimal resemblance to the best-fit line in Figure 4.4. In both, we must add some detector noise (properly scaled to account for the arrival of multiple photoelectrons) on top of the individual hits observed, muddying the overall results. This is particularly important in the latter plot where we expect the kpps rates to drop steeply with increasing star magnitude. There is some evidence of a sharp increase in the kpps rate toward lower magnitudes (brighter stars) that might follow a $-8/5$ slope if we ignore the plot above $m_V \approx 7$; it is conceivable that the line would fit if we removed the detector noise.

To that end, and in general to better understand the OSETI box (for we still have no explanation for the attenuation of signals within the circuit), we add to our list of recommendations that Princeton make some observations of detector noise, both in terms of the kpps numbers and in terms of overall hit rates to see if the detector is capable of producing a background of good hits. Though it is a shame that the hits recorded by Princeton between November 2001 and April 2002 can never be examined for potential coincidences with hits at Harvard, the author is glad that this thesis helped uncover the irregularities at Harvard. Now that the system there is being put in order, the two telescopes should truly be able to observe in tandem.

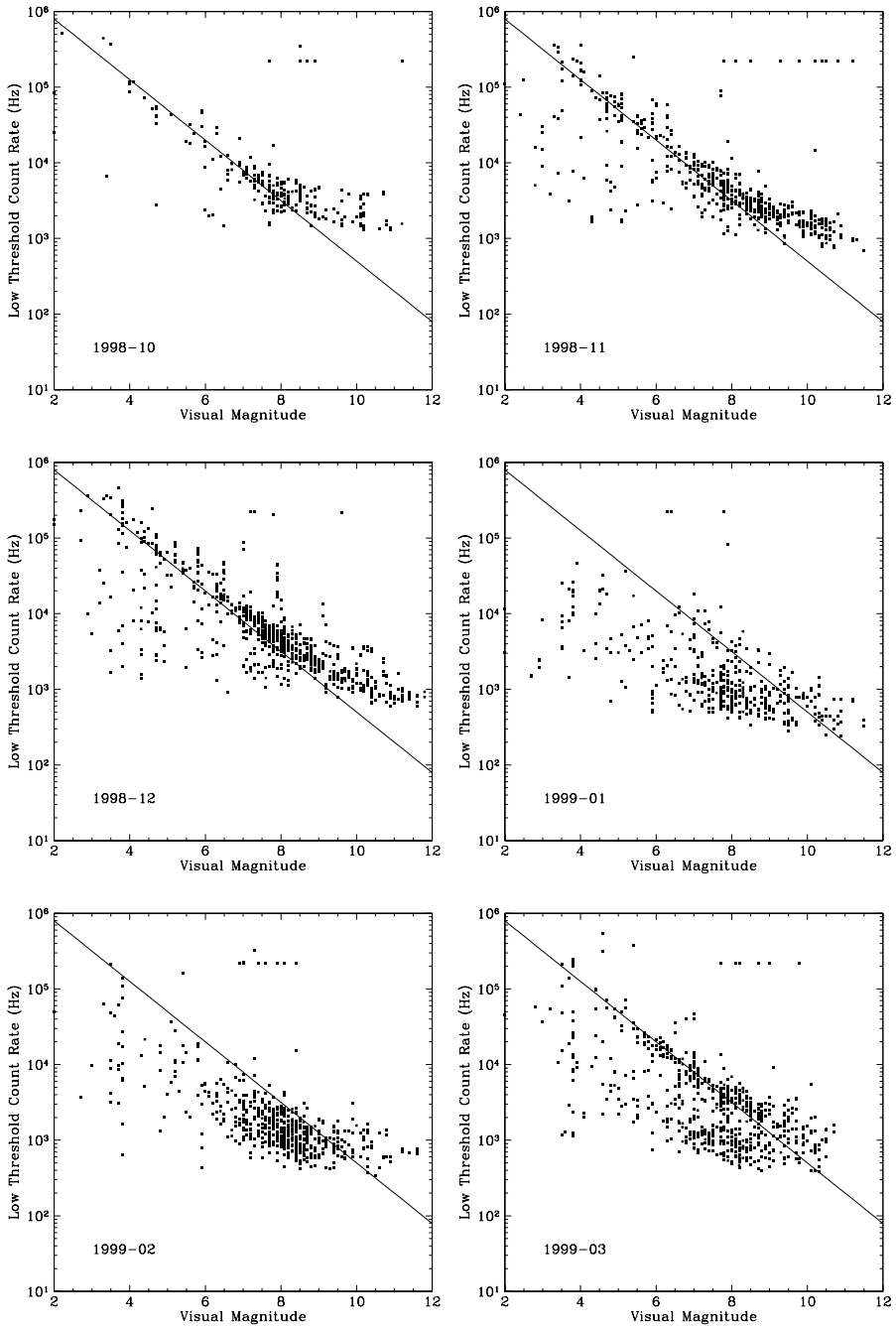

Figure B.1: Kpps rates at Harvard by month from October 1998 to March 1999; note the month and year given in the lower left of each plot. Rates are given in Hz, not kHz. The line plotted on top of these six graphs and in all the following figures has the expected $-2/5$ slope (see Figure 4.1), but the intercept has been changed to reflect the the Oak Ridge telescope's larger area. Plots generated by C. Coldwell, late April 2002 [12].

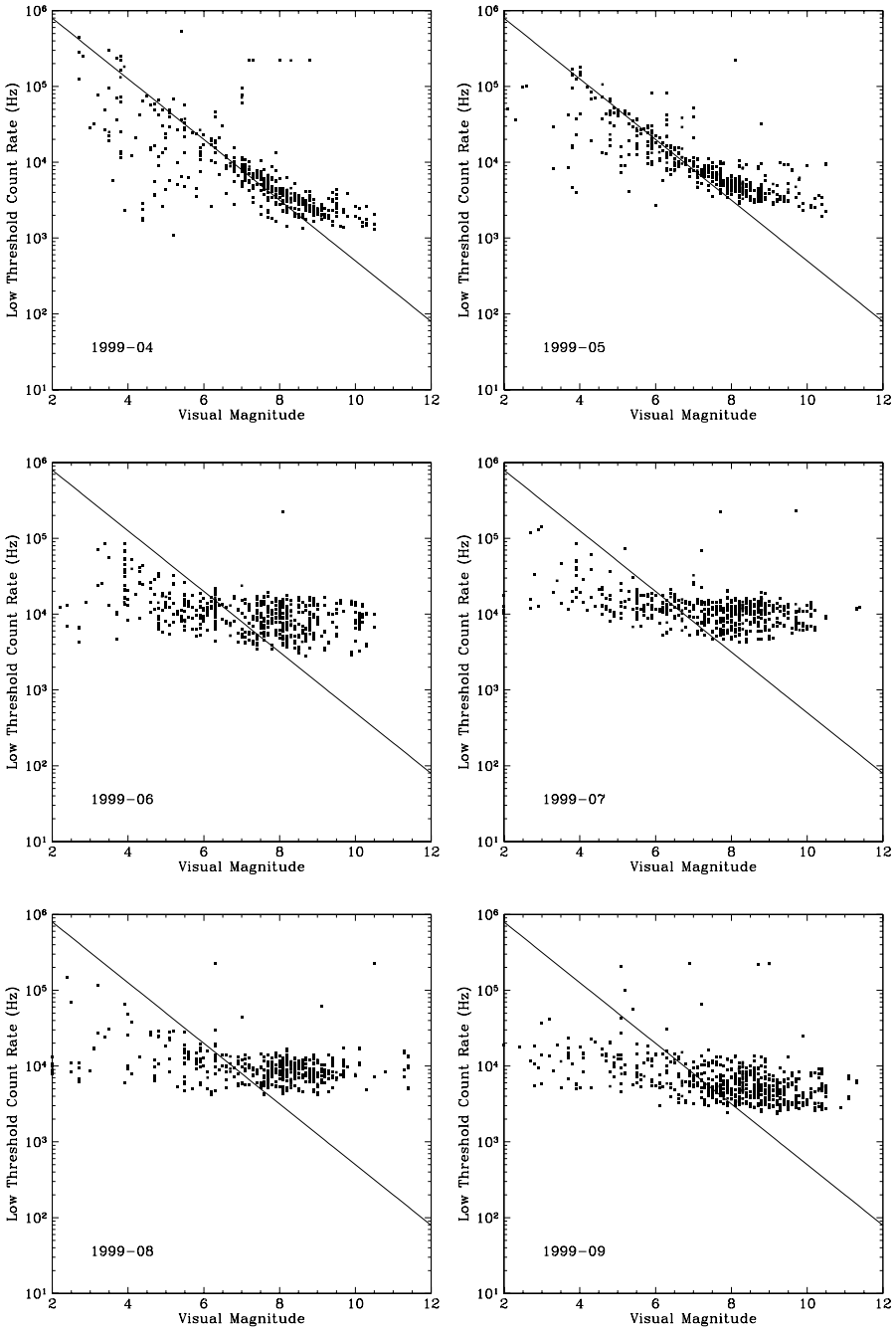

Figure B.2: Kpps rates at Harvard by month from April 1999 to September 1999. The rates are given in counts per second. Plots generated by C. Coldwell, late April 2002 [12].

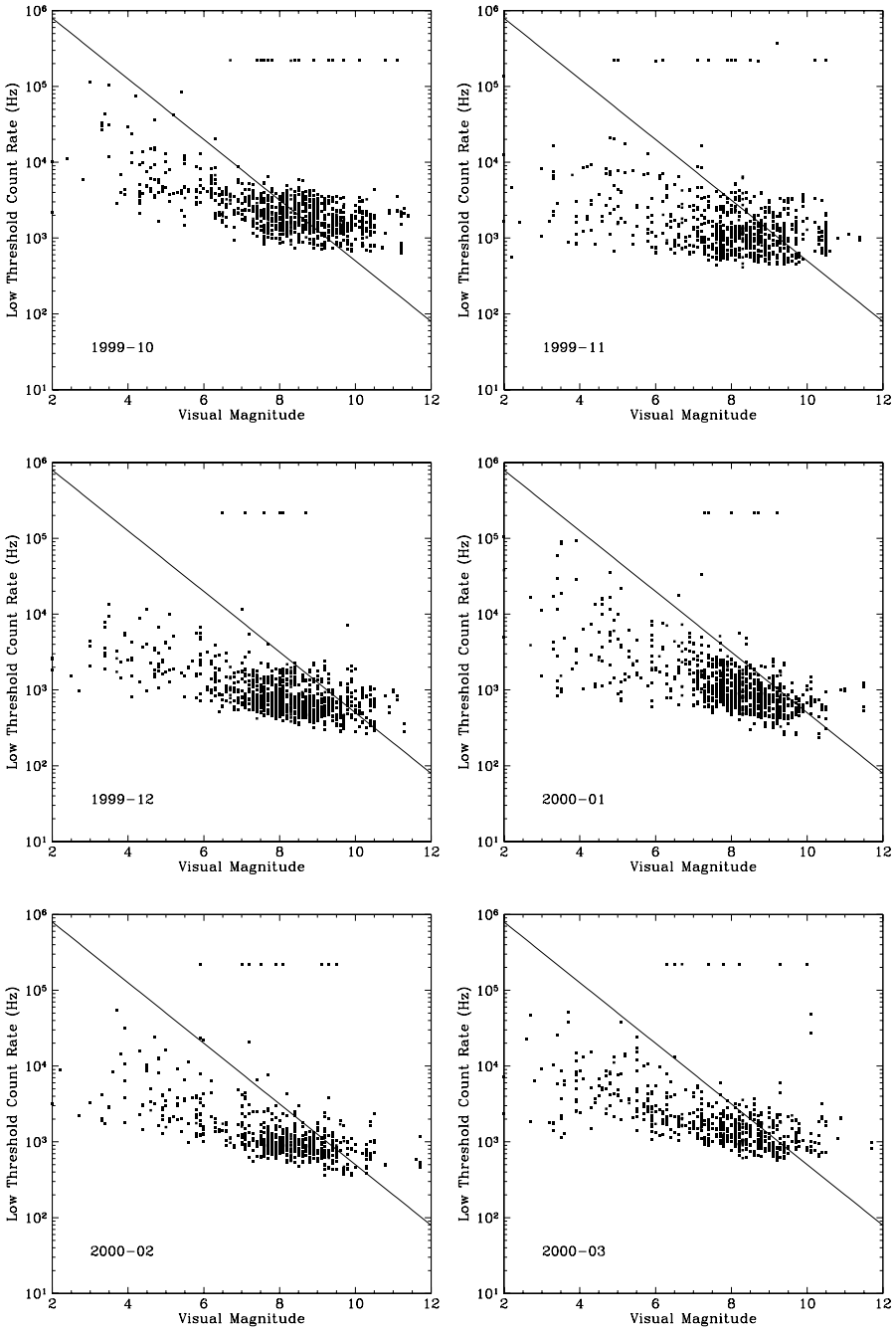

Figure B.3: Kpps rates at Harvard by month from October 1999 to March 2000. The rates are given in counts per second. Plots generated by C. Coldwell, late April 2002 [12].

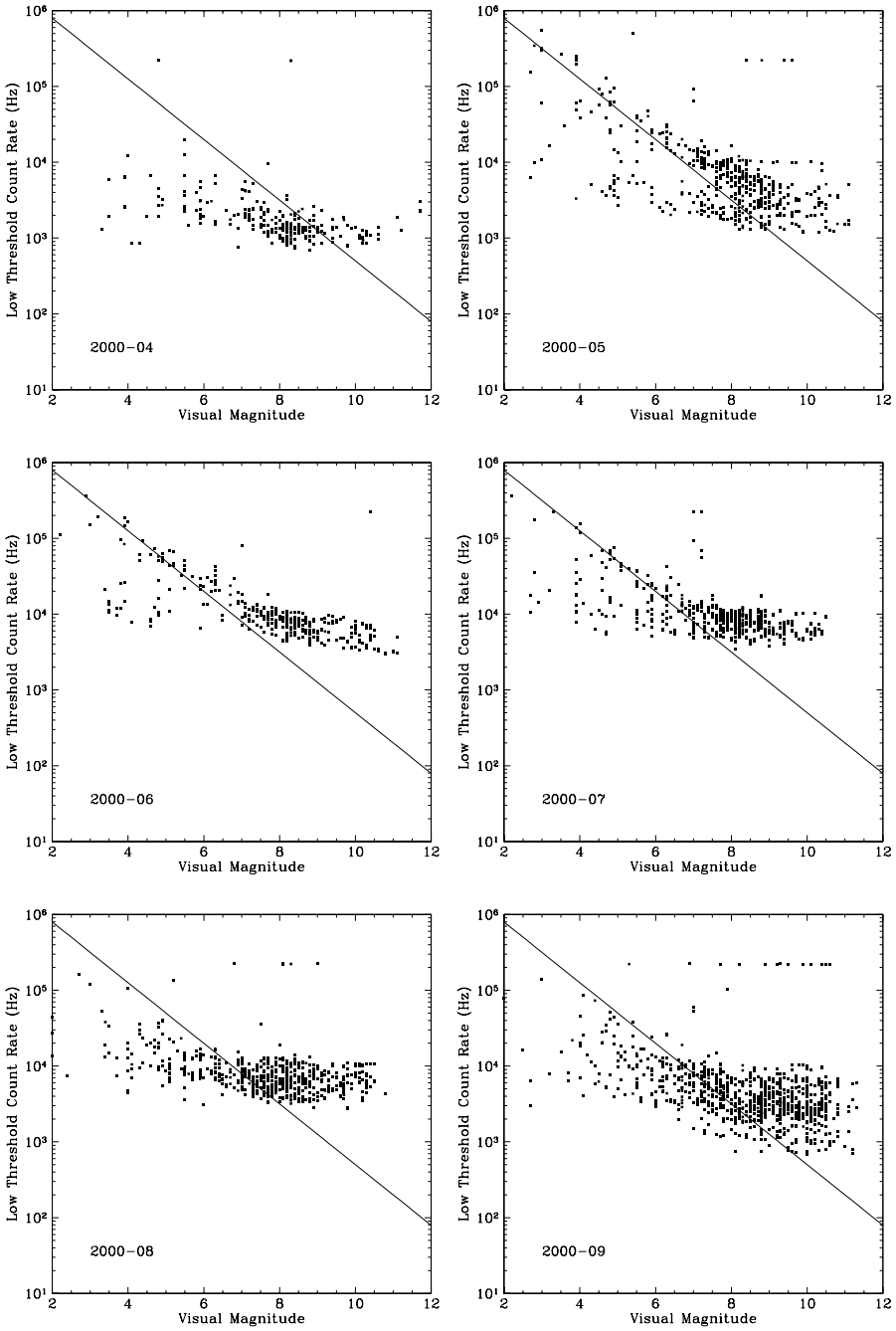

Figure B.4: Kpps rates at Harvard by month from April 2000 to September 2000. The rates are given in counts per second. Plots generated by C. Coldwell, late April 2002 [12].

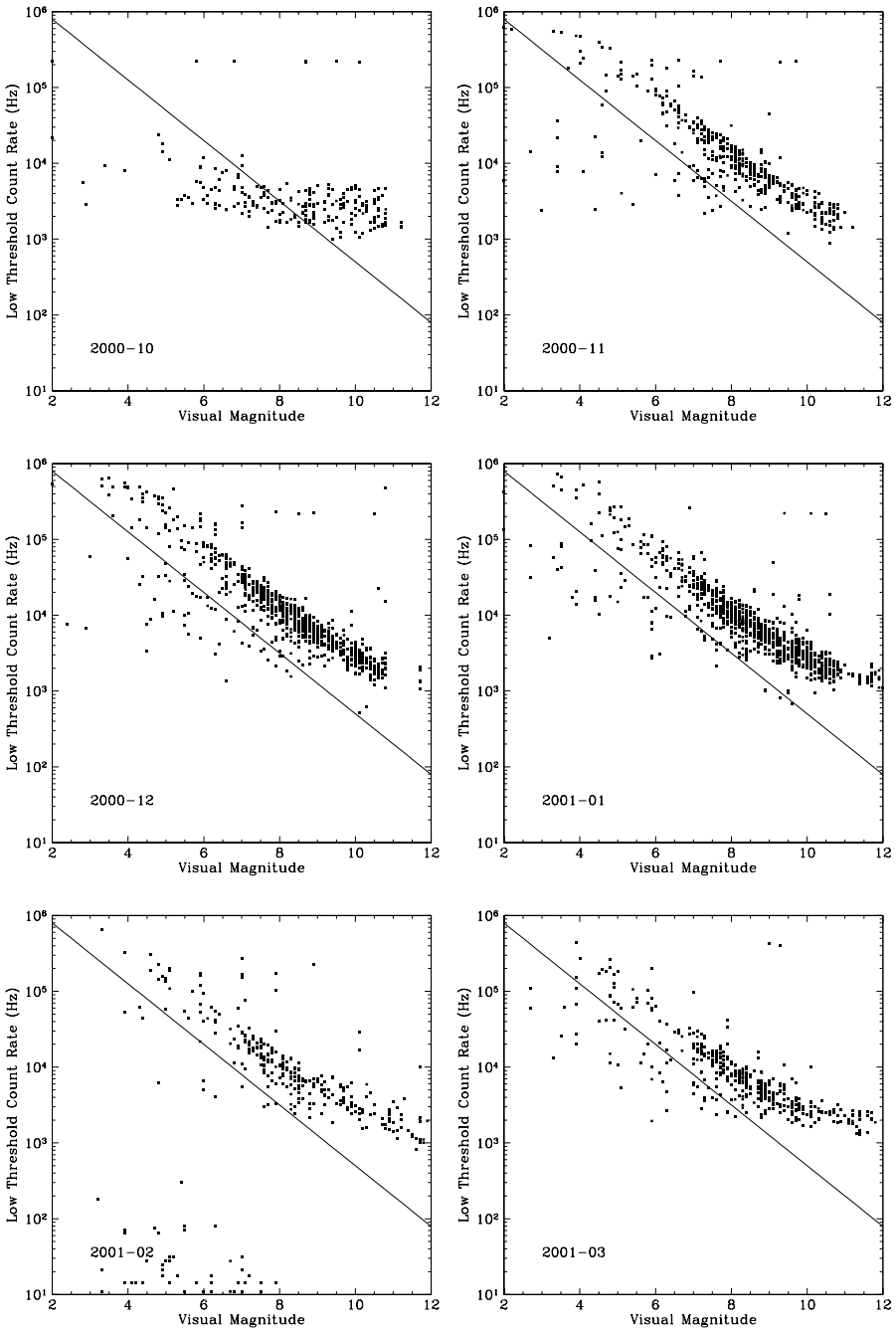

Figure B.5: Kpps rates at Harvard by month from October 2000 to March 2001. The rates are given in counts per second. Plots generated by C. Coldwell, late April, 2002 [12].

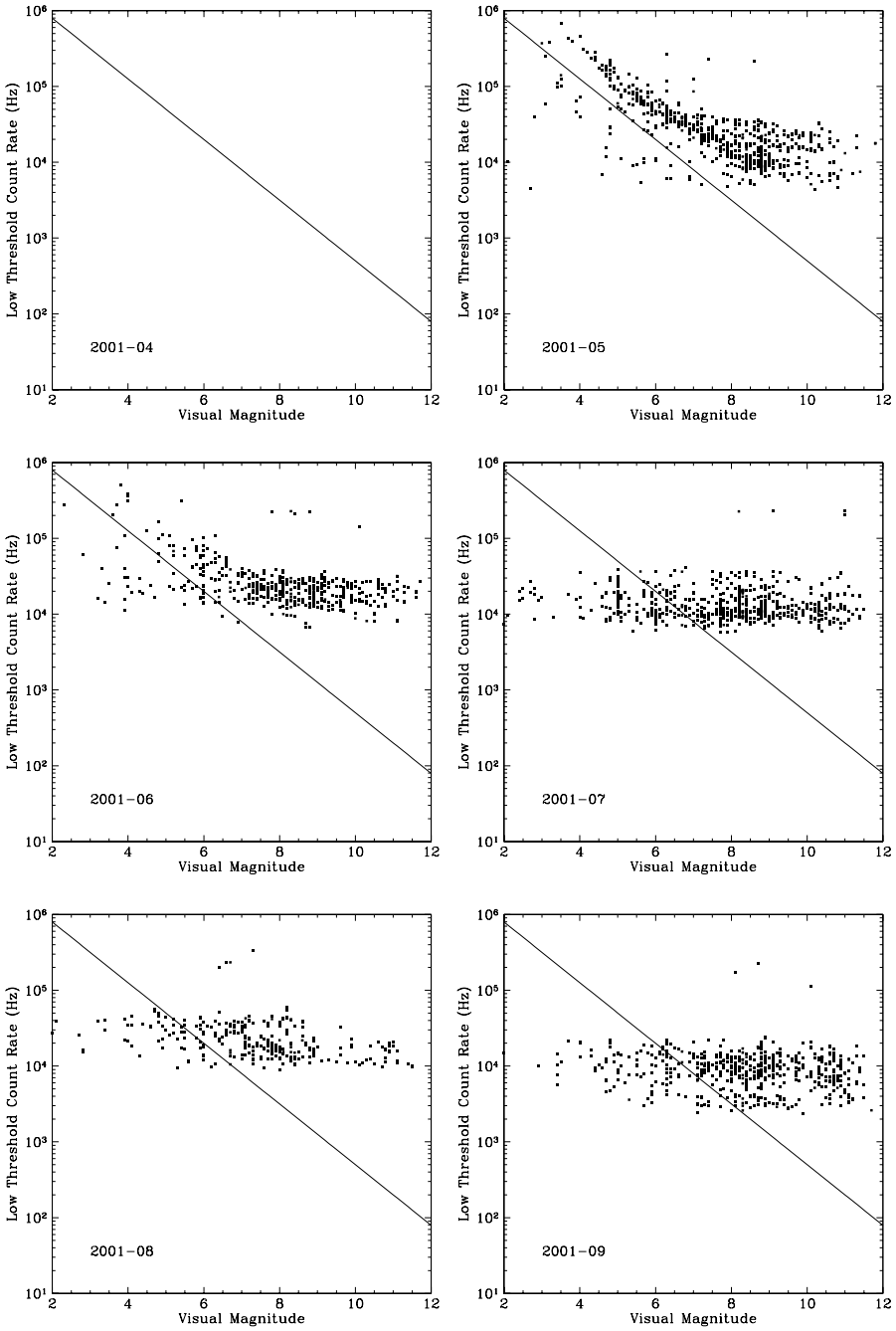

Figure B.6: Kpps rates at Harvard by month from April 2001 to September 2001. The rates are given in counts per second. Plots generated by C. Coldwell, late April 2002 [12].

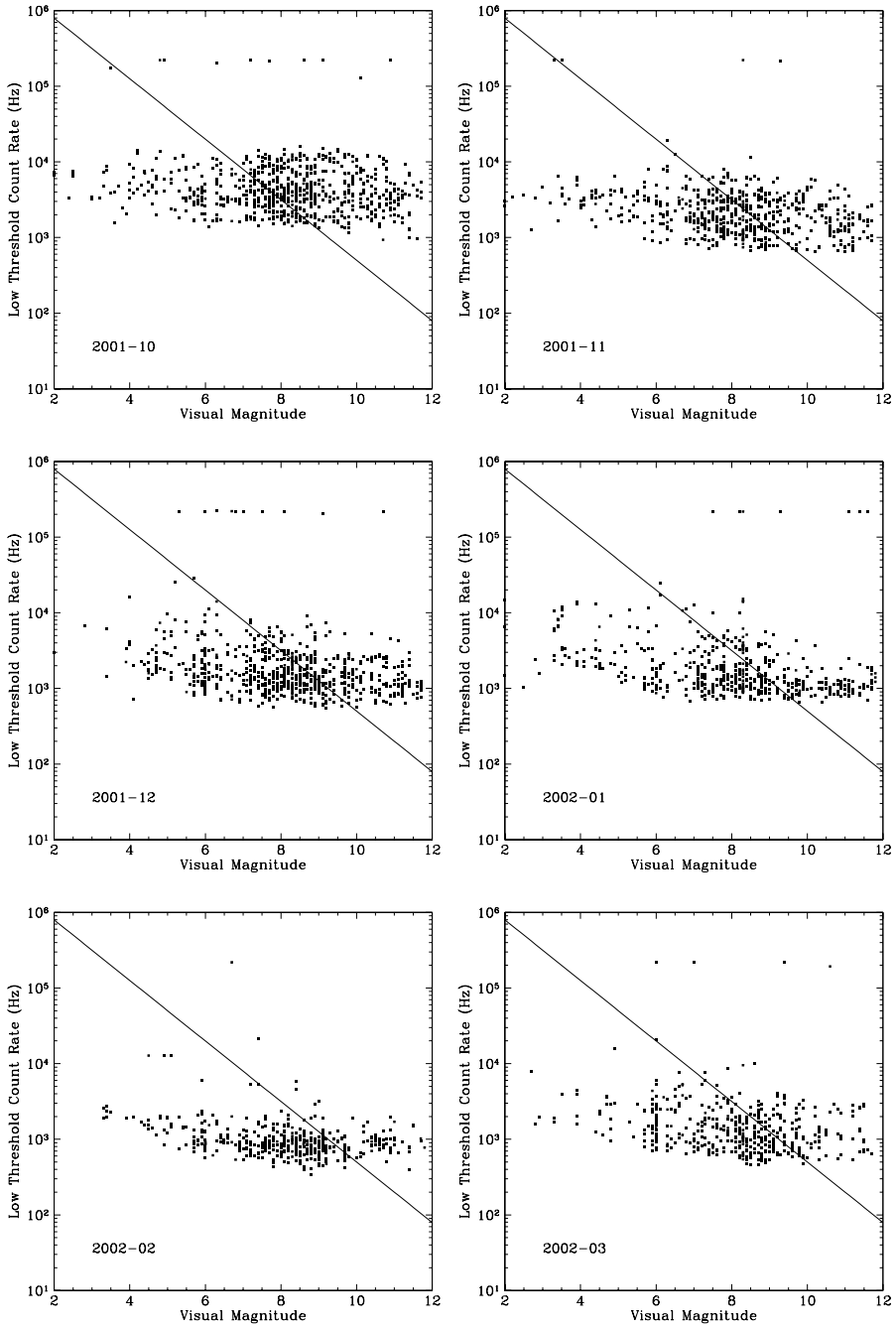

Figure B.7: Kpps rates at Harvard by month from October 2001 to March 2002. The rates are given in counts per second. Plots generated by C. Coldwell, late April 2002 [12].

Bibliography

[1] Fred C. Adams. Modes of star formation and constraints on the birth aggregate of our solar system. In *The Origins of Stars and Planets: The VLT View*. European Southern Observatory, 2001. Preprint as of April 2002: http://www.eso.org/gen-fac/meetings/starplanet2001/proceed.html.

[2] C.W. Allen. *Astrophysical Quantities*, pages 6–8, 277–282. The Athlone Press, London, 3rd edition, 1973.

[3] M.J. Benacquista. Relativistic binaries in globular clusters. *Living Rev. Relativity*, 5(2), 2002. [Online article]: Cited 20 April 2002 at http://www.livingreviews.org/Articles/Volume5/2002-2benacquista/.

[4] Sidney van den Bergh. Globular clusters—a provocative introduction. In *Structure and Dynamics of Globular Clusters*, volume 50 of *A[stronomical] S[ociety of the] P[acific] Conference Series*, 1993.

[5] A. Betz. A directed search for extraterrestrial laser signals. *Acta Astronautica*, 13(10):623, 1986.

[6] James Binney and Michael Merrifield. *Galactic Astronomy*. Princeton University Press, Princeton, 1998.

[7] James Binney and Scott Tremaine. *Galactic Dynamics*, pages 489–493. Princeton University Press, Princeton, 1987.

[8] G. Cocconi and P. Morrison. Searching for interstellar communications. *Nature*, 184:844, 1959.

[9] C. Coldwell. Derivation of the Poisson formula and photon pileup in the OSETI detectors. Private communication; file-name: poisson.ps, 21 February 2002.

[10] C. Coldwell. misaligned. Private communication via e-mail, 7 May 2002.

[11] C. Coldwell. Re: A couple oseti questions. Private communication via e-mail, 26 January 2002.

[12] C. Coldwell. Re: academic responsibility. Private communication via e-mail, 29 April 2002.

[13] C. Coldwell. Re: diagnostic tests. Private communication via e-mail, 15 March 2002.

[14] C. Coldwell. Re: good hit criterion. Private communication via e-mail, 4 April 2002.

[15] C. Coldwell. Re: kpps rate sanity check. Private communication via e-mail, 17 April 2002.

[16] C. Coldwell. Re: That is so bizarre! Private communication via e-mail, 30 April 2002.

[17] C. Coldwell. Re: timestamp, etc. Private communication via e-mail, 6 February 2002.

[18] Arthur N. Cox, editor. *Allen's Astrophysical Quantities*, chapter 22. AIP Press/Springer–Verlag, New York, 4th edition, 2000.

[19] F.D. Drake. The Drake Equation. SETI Institute at http://www.Sseti-inst.edu/science/drake-bg.html, 20 March 2002.

[20] David Halliday, Robert Resnick, and Jearl Walker. *Fundamentals of Physics, Extended*. John Wiley & Sons, Inc., New York, 4th edition, 1993.

[21] Hamamatsu Photonics K. K. Compact hybrid photo-detector: R7110u-07. http://www.hamamatsu.com, Sept 2000.

[22] P. Horowitz. The Technical Case for Optical and Infrared seti. Harvard OSETI at http://seti.harvard.edu/OSETI/tech.pdf, 1998.

[23] P. Horowitz et al. Targeted and All-Sky Search for Nanosecond Optical Pulses at Harvard–Smithsonian. *SPIE Proc.*, 4273, 2001. Also online at http://seti.harvard.edu/OSETI/oseti.pdf.

[24] Kenneth Janes and David Adler. Open clusters and galactic structure. *Astrophysical Journal Supplement*, 49:425, 1982.

[25] William J. Kaufman III and Robert A. Freedman. *Universe*. W.H. Freeman and Company, New York, 5th edition, 1999.

[26] Charles Kittel and Herbert Kroemer. *Thermal Physics*, pages 453–455. W.H. Freeman and Company, New York, 2nd edition, 2000.

[27] Kenneth R. Lang. *Astrophysical Data: Planets and Stars*, chapter 16. Springer–Verlag, New York, 1992.

[28] D.W. Latham. Harvard Spectroscopy Project. Private communication, 2001.

[29] LeCroy Corporation. Lecroy models MTD133b and MTD135 8-channel time-to-digital converter monolithic. LeCroy Corporation at http://www.lecroy.com/lrs/dsheets/mtd.htm, 3 April 2002.

[30] William Mendenhall and Richard L. Schaeffer. *Mathematical Statistics with Applications*, pages 81–85. Duxbury Press, North Scituate, MA, 1973.

[31] Berkeley Optical SETI at the University of California. http://seti.ssl.berkeley.edu/opticalseti/, 25 April 2002.

[32] R.N. Schwartz and C.H. Townes. Interstellar and interplanetary communication by optical masers. *Nature*, 190:205, 1961.

[33] Students for the Exploration and Development of Space. Messier object 13.

[34] C.H. Townes. At what wavelengths should we search for signals from extraterrestrial intelligence? *Proc. Natl. Acad. Sci USA*, 80:1147, 1983.

[35] C.H. Townes. Infrared SETI. *SPIE Proc.*, 1867, 1993.

[36] D.T. Wilkinson. Private communication, 2001 through 2002.

[37] D.T. Wilkinson. *OSETI/Telescope Observer's Manual.* Fitz-Randolph Telescope, Princeton University, Fall 2001.